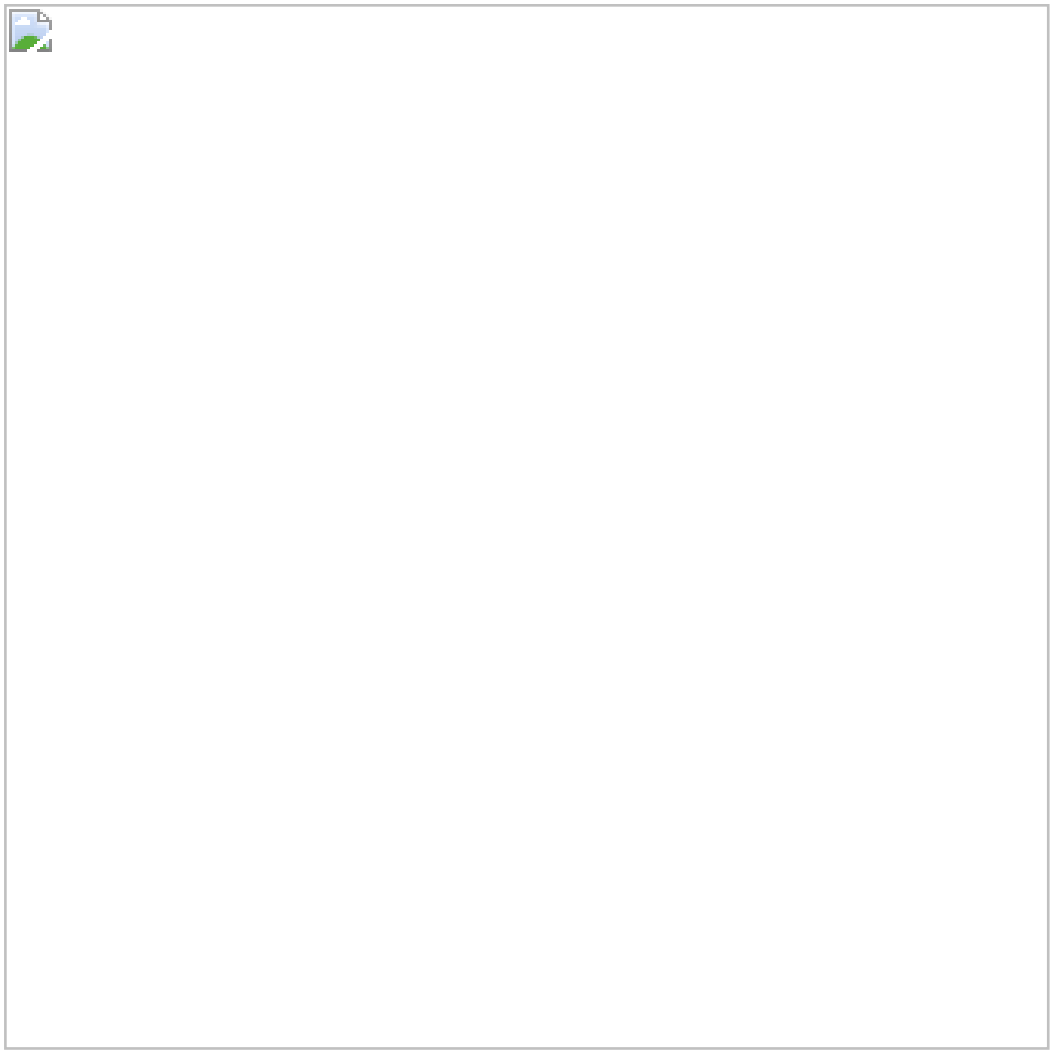

Paternal obesity induces placental hypoxia and sex-specific impairments in placental vascularization and offspring metabolism†

Authors: Jazwiec, Patrycja A., Patterson, Violet S., Ribeiro, Tatiane A., Yeo, Erica, Kennedy, Katherine M., et al.

Source: Biology of Reproduction, 107(2) : 574-589

Published By: Society for the Study of Reproduction

URL: https://doi.org/10.1093/biolre/ioac066

Biology of Reproduction, 2022, **107(2)**,574–589
https://doi.org/10.1093/biolre/ioac066
Advance access publication date 4 April 2022
Research Article

Paternal obesity induces placental hypoxia and sex-specific impairments in placental vascularization and offspring metabolism†

Patrycja A. Jazwiec[1,‡], Violet S. Patterson[1,‡], Tatiane A. Ribeiro[1,2,3,‡], Erica Yeo[1,2], Katherine M. Kennedy[1,2], Paulo C.F. Mathias[3], Jim J. Petrik[4] and Deborah M. Sloboda[1,2,5,6,*]

[1]Department of Biochemistry and Biomedical Sciences, McMaster University, Hamilton, Canada
[2]Farncombe Family Digestive Health Research Institute, McMaster University, Hamilton, Canada
[3]Department of Biotechnology, Genetics and Cell Biology, State University of Maringá, Paraná, Brazil
[4]Department of Biomedical Sciences, University of Guelph, Guelph, Canada
[5]Department of Pediatrics, McMaster University, Hamilton, Canada
[6]Department of Obstetrics and Gynecology, McMaster University, Hamilton, Canada

***Correspondence**: McMaster University, Department of Biochemistry and Biomedical Sciences, 1280 Main St West, Hamilton L8S 4L8, Canada. Tel: +1-905-525-9140; Fax: +1-905-522-9033; E-mail: sloboda@mcmaster.ca

†**Grant Support:** DMS is supported by a Tier 2 Canada Research Chair in Perinatal Programming. PAJ is supported by a Thomas Neilson Scholarship, Fred & Helen Knight Enrichment Award, and an Ontario Graduate Scholarship. TAR was supported by CNPq – Conselho Nacional de Desenvolvimento Científico e Tecnológico – Brasil. EY and KMK are supported by the Farncombe Digestive Health Research Institute Student Fellowship.

‡Authors have equally contributed to the study and are listed in alphabetical order.

Abstract

Paternal obesity predisposes offspring to metabolic dysfunction, but the underlying mechanisms remain unclear. We investigated whether this metabolic dysfunction is associated with changes in placental vascular development and is fueled by endoplasmic reticulum (ER) stress-mediated changes in fetal hepatic development. We also determined whether paternal obesity indirectly affects the *in utero* environment by disrupting maternal metabolic adaptations to pregnancy. Male mice fed a standard chow or high fat diet (60%kcal fat) for 8–10 weeks were time-mated with female mice to generate pregnancies and offspring. Glucose tolerance was evaluated in dams at mid-gestation (embryonic day (E) 14.5) and late gestation (E18.5). Hypoxia, angiogenesis, endocrine function, macronutrient transport, and ER stress markers were evaluated in E14.5 and E18.5 placentae and/or fetal livers. Maternal glucose tolerance was assessed at E14.5 and E18.5. Metabolic parameters were assessed in offspring at ∼60 days of age. Paternal obesity did not alter maternal glucose tolerance but induced placental hypoxia and altered placental angiogenic markers, with the most pronounced effects in female placentae. Paternal obesity increased ER stress-related protein levels (ATF6 and PERK) in the fetal liver and altered hepatic expression of gluconeogenic factors at E18.5. Offspring of obese fathers were glucose intolerant and had impaired whole-body energy metabolism, with more pronounced effects in female offspring. Metabolic deficits in offspring due to paternal obesity may be mediated by sex-specific changes in placental vessel structure and integrity that contribute to placental hypoxia and may lead to poor fetal oxygenation and impairments in fetal metabolic signaling pathways in the liver.

Summary Sentence
Paternal obesity induces placental hypoxia, impairs blood vessel integrity, and is associated with changes in fetal hepatic development, underpinning postnatal metabolic compromised in offspring.

Keywords: hypoxia, metabolism, offspring, paternal obesity, placenta

INTRODUCTION

As of 2016, 13% of adults worldwide were classified as obese [1], increasing their risk of co-morbidities, including coronary heart disease and type 2 diabetes. Obesity risk has traditionally been explained by genetic predisposition and/or lifestyle factors, and the contribution of the early life environment often goes unrecognized [2]. At least some portion of an individual's health trajectory is determined early in life, beginning prior to conception (in germ cells) and continuing into the embryonic, fetal, and early postnatal periods [3]. Early in development an organism responds to environmental signals that change its developmental trajectory [3]. One of the most studied early life signals is fetal exposure to maternal obesity. Although the relationship between maternal obesity, offspring obesity, and metabolic dysfunction is well-established [4, 5], whether the paternal lineage shares a similar contribution is unknown and been largely overlooked and understudied.

Some clinical data exist demonstrating a link between paternal diet and/or obesity, and offspring obesity risk and metabolic dysfunction [6]. Rodent models of paternal diet-induced obesity show impaired offspring glucose regulation [7, 8] and altered mitochondrial function [9], but which specific metabolic organs/pathways are impacted and when, remains unclear. Furthermore, paternal obesity impacts offspring in a sex-specific manner, where females appear to be more vulnerable to paternal lineage-induced early life adversity. In mice, female embryos derived from obese

Received: October 5, 2021. **Revised:** January 31, 2022. **Editorial decision:** March 25, 2022

males have delayed development, and far fewer of them reach the blastocyst stage [10]. In experimental studies, these impairments in embryonic and offspring development have largely been attributed to the damaging effects of paternal obesity on sperm [11–13], and on sperm DNA methylation [14], chromatin structure, and non-coding RNAs [8, 15].

Despite the fact that the sperm epigenome contributes to the growth and development of the placenta [16], few studies have investigated the impact of paternal obesity on placental development [17–19]. None have investigated whether placental changes influence maternal metabolic adaptation to pregnancy. Thus, whether paternal obesity channels indirect effects on the developing fetus/offspring through either maternal metabolic impairments, or through the placenta, is virtually unknown. Although we know that maternal obesity impairs placental vascularization [4, 20], induces hypoxia, oxidative stress [4, 21], endoplasmic reticulum (ER) stress [22], and alters fetal metabolic development [23] in humans and rodents alike, little to no data exist regarding the impacts of paternal obesity on the placenta, or on maternal or fetal metabolic development.

We investigated the impacts of paternal obesity on placental vascular development and the mediating role of cellular stress (ER stress) in a mouse model of high-fat diet-induced obesity. We hypothesized that paternal obesity results in placental ER stress, which impairs placental growth and vascular development, and that these placental changes impair fetal hepatic metabolism, which would be associated with metabolic dysfunction in offspring, including changes to whole body metabolism.

Materials and methods

Animal model

Diet-induced obesity in male mice

All animal experiments were approved by the Animal Research Ethics Board (Animal Utilization Protocol 16-09-35) at McMaster University and were in accordance with the Canadian Council on Animal Care guidelines. We used a model of high fat (HF) diet-induced obesity in C57BL/6 J male mice (Supplemental Figure S1). Six-week-old male mice were randomized to either: 1) *Control (CON) group*: fed a standard chow diet ($n = 49$; 17% kcal fat, 54% kcal carbohydrates, 29% kcal protein, 3 kcal/g; Harlan 8640 Teklad 22/5 Rodent Diet) or 2) *Paternal High Fat (PHF) group*: fed a HF diet ($n = 61$; 20% kcal protein, 20% kcal carbohydrates, 60% kcal fat, 5.21 kcal/g; Research Diets Inc. D12492) *ad libitum* with free access to water for 8–10 weeks. All male mice were housed in the same room at 22 °C and a 12-hour (h) light, 12-h dark cycle. Food intake and body mass were measured weekly. Body adiposity was assessed using a body composition analyzer (Bruker Minispec LF90-II) prior to diet randomization (baseline or 0 weeks), and 5 and 7 weeks after the respective diets. To assess glucose tolerance, a standard intraperitoneal (*i.p.*) glucose tolerance test (GTT) was performed on 12-h fasted male mice at baseline and after 5 weeks of diet consumption. CON and PHF male mice were injected with glucose (G5767; Sigma-Aldrich; 2 g/kg, *i.p.*). Blood glucose was repeatedly measured through tail vein sampling using a commercial blood glucometer (Accu-Check Aviva Roche Diagnostics) prior to glucose injection (0) and at 20, 30, 40, 60, 90, and 120 minutes (min) after glucose injection [24].

Timed mating and pregnancy

After 8–10 weeks of CON or PHF diet, male mice were timed-mated with virgin C57BL/6J female mice. One or two female mice were housed in the same cage with a male mouse overnight. Mating was confirmed by the presence of a copulation plug the following morning and designated at embryonic day (E) 0.5. Pregnant female mice were housed individually and fed a standard chow diet (17% kcal fat, 54% kcal carbohydrates, 29% kcal protein, 3 kcal/g; Harlan 8640 Teklad 22/5 Rodent Diet) *ad libitum* and provided free access to water throughout gestation. Food intake and body mass was measured throughout gestation. Pregnant mice either underwent glucose tolerance testing (see Methods below) or were sacrificed at mid-gestation (E14.5; $n = 10$) or late gestation (E18.5; $n = 10$–13) by cervical dislocation. During placental tissue collection, maternal myometrial tissue was removed so that placental tissue (in the mouse this comprises a junctional zone and labyrinth zone) was separated from the decidua. Placental and fetal liver samples were collected from one randomly selected male and one female fetus in each litter at E14.5 and E18.5 (see Methods below). Fetal tails were collected to identify the sex of the feto-placental units; DNA was extracted from fetal tail samples, and the presence of the *Sry* gene was identified with PCR through-amplification using 5' TTGTCTAGAGAGCATGGAGGGCCATGTC 3′ and 5'CCACTCCTCTGTGACACTTTAGCCCTCCG 3′ primers.

For offspring studies, a separate cohort of pregnant female mice was allowed to deliver and at birth, litters were standardized six pups (three male pups and three female pups) to ensure standardized nutrition during lactation. Offspring food intake and body mass were measured weekly. Male and female CON and PHF offspring were subjected to metabolic assessments (see Methods below) as young adults at postnatal day 53 (P53) and P60, after which they were sacrificed by cervical dislocation at P67.

Maternal glucose assessments

To test whether paternal obesity impacted maternal metabolic adaptations to pregnancy, separate cohorts of pregnant females were subjected to a glucose tolerance test (GTT) at mid-gestation (E14.5, $n = 10$ per group), and term gestation (E18.5, $n = 10$–13 per group). Dams mated with CON and PHF males were fasted for 6 h prior to a GTT. At E14.5, glucose was administered via intraperitoneal (*i.p.*) injection of glucose (G5767; Sigma-Aldrich; 1.5 g/kg). Due to the difficulty of *i.p.* injection with a full gravid uterus at term, glucose was orally administered to E18.5 pregnant dams by gavage (G5767; Sigma-Aldrich; 2 g/kg). At both timepoints, maternal blood glucose was repeatedly measured through tail vein sampling using a commercial blood glucometer (an Accu-Check Aviva Roche Diagnostics) prior to glucose administration (0) and 15, 20, 30, 40, 60, 90, and 120 min after glucose administration.

Offspring metabolic assessments

Metabolic profiling was performed on male and female CON ($n = 14$/sex) and PHF ($n = 8$/sex) offspring using a Comprehensive Lab Animal Monitoring System (CLAMS; Columbus Instruments) at P53 [25], which monitors the mice and records a number of outcome measures. Offspring were placed into individual CLAMS cages at 15:00 h and acclimatized for 24 h prior to acquiring measurements. These included: food

consumption, total horizontal motor activity, heat production, oxygen consumption (VO_2), carbon dioxide production (VCO_2), respiratory exchange ratio (RER), carbohydrate oxidation (carbOx), and lipid oxidation (lipOx). Measurements were acquired every 20 min for 48 h.

At P60, a standard *i.p.* GTT was performed on fasted male and female CON ($n = 6$/sex) and PHF ($n = 7$–8/sex) offspring. Offspring were injected with glucose (G5767; Sigma-Aldrich; 2 g/kg, *i.p.*) and blood glucose was repeatedly measured through tail vein sampling using a commercial blood glucometer (an Accu-Check Aviva Roche Diagnostics) prior to glucose injection (0) and 20, 30, 40, 60, 90, and 120 min after glucose injection.

Insulin ELISAs

Serum insulin concentrations were quantified using a commercially available insulin immunoassay kit (32380; Toronto Bioscience) as per manufacturer's instructions using a Synergy H4 Hybrid microplate reader (BioTek Instruments). Insulin concentrations were interpolated from a standard curve determined by curve of 4-parameter as per manufacturer's instructions. Homeostatic model assessment of insulin resistance (HOMA-IR) was calculated by multiplying blood glucose concentrations (mmol/L) by serum insulin concentrations (mU/mL), and dividing this value by 22.5 [26].

Molecular analyses

RNA extraction and complementary DNA synthesis

Placentae and livers from one randomly chosen male and one female fetus were collected from each pregnancy per sire and homogenized in TRIzol reagent (15596018; Invitrogen) using glass homogenizing beads (10064583; ACROS Organics) and a homogenizer (MP116004500; MP Biomedicals). Homogenates were centrifuged at 12 000 *g* for 10 min at 4 °C. Supernatant was removed, added to chloroform (BP1145-1; FisherBioReagents), and thoroughly mixed. Samples were incubated at room temperature (RT) for 3 min, and centrifuged 12 000 *g* for 10 min at 4 °C. The aqueous layer was removed, mixed with isopropanol (BP26181; FisherBioReagents), incubated at RT for 20 min, and then centrifuged at 12 000 *g* for 10 min at 4°C. Supernatant was removed, the remaining RNA pellets were washed twice in 75% ethanol (EtOH), and then reconstituted in 20 μL of ultrapure water (UP-H_2O). RNA was quantified using a NanoDrop 2000 spectrophotometer (ThermoScientific). RNA quality was determined using ratio of absorbance at 260:280 nm (A_{260}/A_{280}) and 260:230 nm (A_{260}/A_{230}). RNA samples with an A_{260}/A_{280} and A_{260}/A_{230} ratio of >2.0 and >1.5, respectively, were used to generate complementary (cDNA). RNA was stored at −80 °C until 2μg of RNA was used for first strand cDNA (cDNA) synthesis using SuperScript IV VILO Master Mix with ezDNase enzyme (11766050; Invitrogen) as per the manufacturer's instructions. Complementary DNA samples were diluted to 1:100 in UP-H_2O and stored at −80 °C until required for quantitative PCR (qPCR) assays.

Quantitative PCR Assays

Quantitative PCR assays were performed as previously described [4]. Primer sets of candidate genes (Supplemental Table S1, S2) were designed using Primer Basic Local Alignment Search Tool (Primer-BLAST) software available at the National Center for Biotechnology Information (https://www.ncbi.nlm.nih.gov/tools/primer-blast/, NCBI). Primer conditions were adjusted to the following cycling conditions: PCR Product Size: min: 50 bp, max: 150 bp; primer melting temperatures (T_m): min: 58 °C, opt: 60 °C, max: 62°C; Max T_m Difference: 2 °C. Primer pairs were designed to span exon–exon junctions. Primers were manufactured by Invitrogen (Invitrogen Life Technologies).

The LightCycler 480 SYBR Green I Master and the LightCycler 480 system (Roche Diagnostics) were used for quantifying transcript levels. Each reaction consisted of cDNA (1:100 dilution), 5 μM forward primer, and 5 μM reverse primer for the gene of interest, ultrapure-H_2O, and Lightcycler 480 SYBR Green I Master (04887352001; Roche Diagnostics). The cycling conditions were enzyme activation at 95 °C for 5 min, amplification of the gene product through 60 successive cycles of 95 °C for 10 s, 60 °C for 10 s, and 72 °C for 10 s, and melting curve beginning at 65 °C and ending at 95 °C. Each qPCR assay contained a standard curve (10-fold serial dilution of pooled cDNA), cDNA of samples, and a non-template control (UP-H_2O). Transcript levels were quantified in triplicate for each standard and sample. Gene expression data were normalized to the geometric mean of at least two housekeeping genes (Supplemental Table S3).

Placental histology

Placental trophoblast giant cells

A subset of placental samples at E14.5 were processed to quantify the number of parietal trophoblast giant cells as a marker of placental lactogen (PL) production. These cells are responsible for the secretion of PL [27], which modulates maternal glucose metabolism. Placental samples were fixed in modified Davidson Fixative (MDF) for 8 h at RT, prior to being processed, paraffin-embedded, and serially sectioned at 8 μm. Three replicate placental sections (including the junctional zone and labyrinth zones) 80 μm apart were stained for polysaccharides (including glycogen) as a marker for giant cells using Periodic Acid Schiff (PAS, 395B-1KT, Sigma-Aldrich) ($n = 7$–11/group/sex). Parietal trophoblast giant cells were counted using Nikon NIS Imaging Analysis Software (v.5.20.02).

Placental immunostaining and histology

To investigate markers of angiogenesis and hypoxia, a subset of E14.5 and E18.5 placentae were immersion-fixed in MDF or in 4% paraformaldehyde (50980486; FisherScientific), respectively. Fixed tissues were paraffin-embedded and serially sectioned at 4 μm. Three replicate sections from each placental sample (which included both the junctional zone and labyrinth zone together as a total) were immunolabeled for: hypoxia marker carbonic anhydrase 9 (CA IX), pro-angiogenic factors vascular endothelial growth factor A (VEGF-A) and vascular endothelial growth factor receptor 2 (VEGFR-2), endothelial cell marker cluster of differentiation 31 (CD31), and pericyte marker α-smooth muscle actin (α-SMA) (antibodies used shown in Supplemental Table S4). Antigen retrieval was performed with 10 mM sodium citrate buffer with Tween at 95 °C for 12 min (pH 6.0, washed 2 x 5 min in TBS). Non-specific binding was blocked with 5% bovine serum albumin (BSA; in TBST pH 7.4, A2153; Sigma-Aldrich). Sections were incubated with primary antibody (diluted in 1% BSA/TBST) in a humidified chamber overnight at 4 °C. Sections were then incubated with a

biotinylated secondary antibody (1:100 dilution in TBST, PK6101; Vector Laboratories) or fluorescently-conjugated secondary antibodies (Sigma-Aldrich, Canada and Vector Laboratories) for 1 h. Sections were counterstained with 4′-6-diamidino-2-2phenylindole (DAPI), and mounted with coverslips using fluorescence mounting media. For chromogenic immunohistochemistry, sections were incubated with an avidin–biotin peroxidase complex following VectaStain ABC kit protocols (PK-4000; Vector Laboratories). Biotinylated antibody was visualized with chromagen development using 3,3′ diaminobenzidine (DAB) peroxidase (SK-4100; Vector Laboratories), then sections were counterstained with Mayer's Hematoxylin (MHS32; Sigma-Aldrich), and mounted with coverslips using Permount Mounting Media (SP15500; FisherScientific).

The proportion of positive immunostaining relative to total placental area (including both the junctional and labyrinth zones) was determined using a threshold for DAB-positive staining or the proportion of fluorescent-positive cells using NIS Elements Software (Nikon Instruments Inc). Image analysis was performed using an Olympus BX-61 microscope and integrated morphometry software (MetaMorph) (CA IX, VEGF-A, and α-SMA) or on a Nikon Eclipse NI microscope and Nikon NIS Elements Imaging Software (v.4.30.02). The ratio of CD31 to α-SMA immunopositive area was used as a marker of vessel integrity. All image analyses were performed by an investigator blinded to the study groups. To investigate the proportion of area that each placental zone (junctional and labyrinth zones) occupied of the total tissue section area in CON and PHF placentae at E14.5 and E18.5, placental sections 80 μm apart were stained using Periodic Acid Schiff (PAS, 395B-1KT, Sigma-Aldrich) ($n = 4$-/group/sex). Image analysis was performed using a Nikon Eclipse NI microscope and Nikon NIS Imaging Analysis Software (v.5.20.02). All image analyses were performed by an investigator blinded to the study groups.

Immunoblotting

Total protein extraction

Placental and fetal hepatic tissues were homogenized in extraction buffer (50 mM HEPES, 150 mM NaCl, 100 mM NaF, 10 mM sodium pyrophosphate, 5 mM EDTA, 250 mM sucrose, 1% Triton-X, 1 mM sodium orthovanadate, 1% protease inhibitor tablet) using ceramic homogenizing beads (19-646-3; Omni International). Total protein concentration was quantified using the Pierce BCA Protein Assay Kit (23225; ThermoFisher Scientific) according to the manufacturer's protocol.

Nuclear protein extraction

Liver tissue was homogenized in hypotonic lysis buffer (10 mM HEPES, pH 7.9, 1.5 mM $MgCl_2 \bullet 6\ H_2O$, 10 mM KCl, 1% protease inhibitor tablet) using ceramic homogenizing beads (19-646-3, Omni International), centrifuged at 11 000 *g* for 20 min, and the supernatant was discarded (cytoplasmic fraction). The pellet (nuclei) was resuspended in extraction buffer (20 mM HEPES, pH 7.9, 1.5 mM $MgCl_2 \bullet 6\ H_2O$, 420 mM NaCl, S671–3, 0.2 mM EDTA, 25% v/v glycerol, 1% protease inhibitor tablet) and homogenized again as described above. Homogenates were incubated at RT for 30 min, centrifuged at 21 000 *g* for 5 min, and nuclear fractions were quantified using the Pierce BCA Protein Assay Kit (23225, ThermoFisher Scientific) as per manufacturer's protocol.

Total and nuclear protein detection

Total and nuclear protein was separated using SDS-PAGE (7.5–15% separating gel). Proteins were transferred to membranes (1620177, BioRad) using a TransBlot Turbo Transfer System (1704150, BioRad). Blots were then blocked in 5% BSA (in TBST, A2153-1KG, Sigma-Aldrich) and incubated overnight in rabbit anti-mouse primary antibody for proteins of interest (Supplemental Table S5) and with horseradish peroxidase-conjugated goat anti-rabbit IgG secondary antibodies (ab6721, Abcam). Proteins of interest were detected using Clarity Western ECL Blotting Substrate (1705061; BioRad) or Clarity Max Western ECL Blotting Substrate (1705062; BioRad) and images were captured using a ChemiDoc MP Imaging System (1708280; BioRad). Densitometric quantification was completed using ImageLab software (ImageLab Software for PC Version 6.0.1 SOFT-LIT-170-9690-ILSPC; Bio-Rad).

Phosphorylated protein detection

Phosphorylated proteins were separated using SDS-PAGE (7.5–15% separating gel), transferred to membranes (1620177, BioRad) using a TransBlot Turbo Transfer System (1704150, BioRad), and blocked in 5% BSA (in TBST, A2153-1KG, Sigma-Aldrich). Blots were incubated overnight in rabbit anti-mouse primary antibody for phosphorylated protein of interest (Supplemental Table S5), then incubated in a horseradish peroxidase-conjugated goat anti-rabbit IgG secondary antibody (ab6721, Abcam). Phosphorylated proteins of interest were detected using Clarity Western ECL Blotting Substrate (1705061; BioRad). Images were captured using a ChemiDoc MP Imaging System (1708280; BioRad). Blots were incubated in stripping buffer (21059, ThermoFisher Scientific), washed twice in TBST, then blocked in 5% BSA (in TBST, pH 7.4, A2153; Sigma-Aldrich). Blots were probed with the rabbit anti-mouse primary antibody binding to the total protein (phosphorylated and unphosphorylated; Supplemental Table S5) protein of interest. Total protein was detected by incubating blots in Clarity Western ECL Blotting Substrate (1705061; BioRad). Images were captured using a ChemiDoc MP Imaging System (1708280; BioRad).

Protein quantification

Total and nuclear protein levels are expressed as fold change relative to loading control β-actin and TBP, respectively. Phosphorylated proteins levels are expressed as a ratio relative to unphosphorylated (total) protein levels. To control for inter-gel variability, protein levels were then normalized to a quality control pool composed of all samples in that gel. All immunoblotting data were analyzed using ImageLab software (Image Lab Software for PC (Version 6.0.1 SOFT-LIT-170-9690-ILSPC).

Statistical analyses

For all pregnancy and offspring analyses, the experimental unit is the sire and the sample size represents the number of litters analyzed. For each analysis, one random male and female fetus/placenta were analyzed from one pregnancy (or litter) that was sired by a CON or PHF male mouse. Therefore, each placental and hepatic sample and each offspring measure, was sired by an individual male and represents a replicate

of one wherever possible. Where one sire impregnated more than one female, all outcomes measures were meaned for litter to account for this. All data (except for metabolic activity in offspring assessed using Comprehensive Lab Animal Monitoring System (CLAMS)) were analyzed either by a Student *t*-test, repeated measures two-way ANOVA or mixed-effects model with paternal diet and time as factors, or two-way ANOVA with paternal diet and feto-placental sex as factors. Bonferroni's post-hoc was used for multiple comparisons where appropriate. Data that were not normally distributed were analyzed using a Mann–Whitney *U* test or Student *t*-test with Welch correction, respectively. All data are presented as mean ± standard error of the mean (SEM) unless otherwise indicated. In all cases, significance (∗) was set at $P < 0.05$. Data were analyzed using GraphPad Prism (GraphPad Prism 6.01 for Windows and GraphPad Prism 8.4.2 for MacOS, GraphPad Software, La Jolla California USA, www.graphpad.com).

Offspring metabolic activity (CLAMS) data were analyzed using linear mixed-effects model (LMM) using the lme4 package (R package, RRID:SCR_015654) with the main effects and multiple comparisons determined by Satterthwaite method of approximation in lmerTest (R package, RRID:SCR_015656). Response variable data were separated into light (7:00 to 19:00) and dark (19:00 to 7:00), and average values were taken for heat production, VO_2, VCO_2, RER, carbOx, and lipOx. Sums were taken for food consumption, and activity. Linear mixed-effects model was performed with time period, mouse sex, and paternal diet as fixed variables, and mouse ID and litter as nested random effects.

Results

Male mice fed a HF diet are obese, glucose intolerant, and insulin resistant

At baseline, prior to diet feeding, fasting blood glucose levels and glucose tolerance were similar between sires randomized to CON or HF diet (Supplemental Figure S2A–C). Consistent with previous work in mice [24], males consuming a HF diet became obese, characterized by increased body mass and body adiposity, compared to CON males (Supplemental Figure S2D and E). After 5 weeks of consuming a HF diet, PHF males were hyperglycemic, glucose intolerant, hyperinsulinemic, and insulin resistant (Supplemental Figure S2F–J). Therefore, PHF males were metabolically compromised prior to mating.

Paternal obesity impairs mating efficiency and does not impact feto-placental growth

Diet-induced obesity in males decreases sperm count and sperm motility, reduces the number of sperm with normal morphology [28], increases sperm oxidative stress-induced DNA damage [29], and is associated with reduced fertility [28]. We found that more male–female pairings were necessary to produce a pregnancy in females mated with PHF males, compared to females mated with CON males ($P = 0.0424$; Figure 1A). We also observed significantly fewer pregnancies generated as a proportion of total copulation plugs in PHF-mated females ($P = 0.0006$; Figure 1B). We observed significantly fewer copulation plugs generated as a proportion of the total number of pairings with PHF males

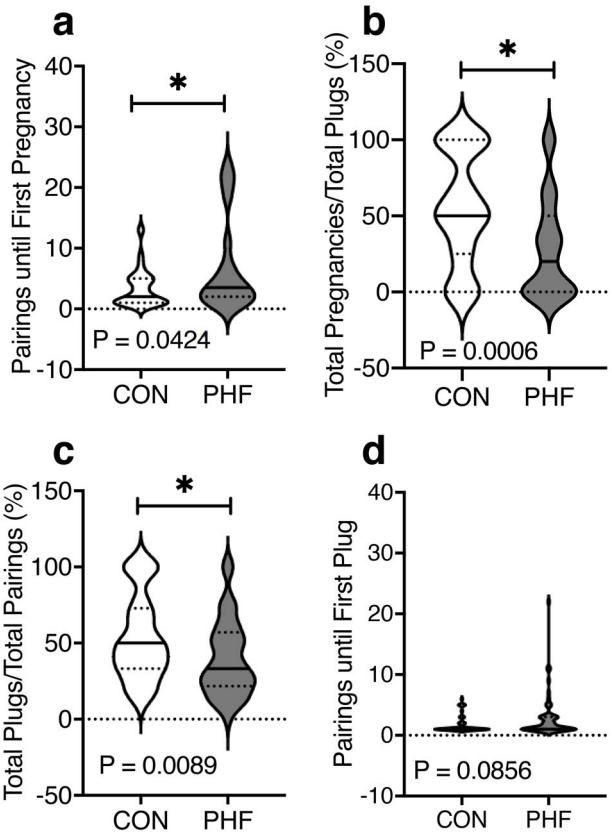

Figure 1. Paternal obesity impairs mating efficiency. CON and PHF males were time-mated with females to generate pregnancies. (a) More mating attempts were necessary to produce a pregnancy in females mated with PHF males compared to females mated with CON males. (b) There were significantly fewer pregnancies generated as a proportion of total copulation plugs in PHF-mated females. (c) Fewer copulation plugs were generated as a proportion of total pairings in PHF-mated females. (d) It took moderately longer for females paired with PHF males to produce a copulation plug compared to those paired with a CON male. CON; $n = 43$–45, PHF; $n = 40$–55. Data are presented as truncated violin plots with the center line representing the median. $*P < 0.05$ compared to CON using Student *t*-test or Mann–Whitney *U* test. CON = Control (open plots); PHF = Paternal high fat diet-induced obesity (gray plots).

($P = 0.0089$; Figure 1C), and it took moderately longer for females paired with PHF males, to produce a copulation plug (Figure 1D), although this difference was not statistically significant ($P = 0.0856$).

Although previous studies show that paternal obesity reduces fertilization success, reduces implantation rate [10], and alters fetoplacental development [10], in our study, litter size, number of resorptions per litter, fetal sex ratio, maternal body mass, and fasting blood glucose levels were similar between CON and PHF pregnancies at E14.5 and E18.5 (Table 1). Placental and fetal body mass were similar between male and female CON and PHF litters at E18.5 (Table 1) as were the areas of the junctional and labyrinth zones, and as proportions of the total placental area (Table 1).

Paternal obesity alters markers of placental angiogenesis and results in placental hypoxia

As angiogenesis is critical for placental vascular development, a process regulated by hypoxia [30], we quantified placental immunostaining of hypoxia marker CA IX, in total placental

Table 1. Maternal and fetal outcomes at mid-gestation (E14.5) and late gestation (E18.5)*

E14.5

Maternal/litter outcomes	**Sire group**				***P*-value**
	CON (n = 25–26)		PHF (n = 19–20)		
Dam gestational mass gained (g)	5.0 ± 0.2		5.0 ± 0.2		0.8328
Dam fasting blood glucose (mmol/L)	5.4 ± 0.2		5.3 ± 0.2		0.9518
Litter size (Fetuses/Litter)	7.4 ± 0.2		7.7 ± 0.2		0.4720
Number of resorptions (Resorptions/Litter)	1.3 ± 0.2		0.8 ± 0.2		0.1660
Fetal sex ratio (Male:Female)	1.5 ± 0.3		1.1 ± 0.3		0.1989
Feto-placental outcome	Male (n = 11–22)	Female (n = 10–22)	Male (n = 7–19)	Female (n = 7–19)	*P*-value or main effect
Fetal body mass (g)	0.247 ± 0.005[a]	0.226 ± 0.005[b]	0.236 ± 0.005[a]	0.228 ± 0.005[a]	P_{Diet} = 0.3874 P_{Sex} = 0.0062 P_{Int} = 0.2246
Placental mass (g)	0.097 ± 0.002	0.092 ± 0.002	0.093 ± 0.002	0.086 ± 0.002	Male:0.0530 Female:0.0530
Feto:Placental ratio	2.577 ± 0.042	2.556 ± 0.055	2.575 ± 0.075	2.706 ± 0.048	Male: 0.5448 Female: 0.0834
Junctional zone area (μm^2)	3102391.97 ± 164857.35	2980740.14 ± 152920.19	3105712.66 ± 124421.81	2732668.80 ± 170987.22	P_{Diet} = 0.4604 P_{Sex} = 0.1409 P_{Int} = 0.4484
Relative junctional zone area (% Total placental area)	46.919 ± 1.671	46.237 ± 1.202	45.377 ± 0.945	43.662 ± 1.996	P_{Diet} = 0.1999 P_{Sex} = 0.4517 P_{Int} = 0.7441
Labyrinth zone area (μm^2)	3485096.06 ± 111125.47	3444137.95 ± 84331.12	3723331.52 ± 48886.97	3498763.54 ± 122712.91	P_{Diet} = 0.1630 P_{Sex} = 0.2046 P_{Int} = 0.3772
Relative labyrinth zone area (% Total placental area)	53.083 ± 1.671	53.763 ± 1.202	54.623 ± 0.945	56.338 ± 1.996	P_{Diet} = 0.1999 P_{Sex} = 0.4517 P_{Int} = 0.7441
Total placental area (μm^2)	6587488.03 ± 164766.62[a]	6424878.09 ± 193723.61[a]	6829044.17 ± 152886.52[a]	6231432.34 ± 157951.19[a]	P_{Diet} = 0.8943 P_{Sex} = 0.0425 P_{Int} = 0.2351

E18.5

Maternal/litter outcomes	**Sire group**				**Main effect**
	CON (n = 17–23)		PHF (n = 12–18)		
Gestational mass gained (g)	14.8 ± 0.5		13.9 ± 0.5		0.2072
Dam fasting blood glucose (mmol/L)	5.0 ± 0.8		4.7 ± 0.6		0.1902
Litter size (Fetuses/Litter)	7.9 ± 0.3		7.5 ± 0.4		0.7046
Number of resorptions (Resorptions/Litter)	0.7 ± 0.2		1.5 ± 0.5		0.1538
Fetal sex ratio (Male:Female)	1.7 ± 0.2		2.1 ± 0.5		0.8504
Feto-placental outcome	Male (n = 4–23)	Female (n = 4–23)	Male (n = 4–18)	Female (n = 4–18)	*P*-value or main effect
Fetal body mass (g)	1.09 ± 0.02	1.06 ± 0.02	1.09 ± 0.02	1.08 ± 0.02	Male: 0.8101 Female: 0.4843
Placental mass (g)	0.093 ± 0.004	0.082 ± 0.003	0.083 ± 0.004	0.086 ± 0.004	P_{Diet} = 0.4045 P_{Sex} = 0.2980 P_{Int} = 0.0689
Feto:Placental ratio	11.89 ± 0.53	13.15 ± 0.66	13.18 ± 0.79	12.83 ± 0.77	P_{Diet} = 0.4776 P_{Sex} = 0.5039 P_{Int} = 0.2432
Junctional zone area (μm^2)	3762725.50 ± 551856.55	3787909.98 ± 302281.50	3332501.32 ± 170759.64	3725924.90 ± 145544.67	P_{Diet} = 0.4754 P_{Sex} = 0.5426 P_{Int} = 0.5916
Relative junctional zone area (% Total placental area)	62.168 ± 3.014	59.855 ± 1.319	59.230 ± 2.555	65.593 ± 2.196	P_{Diet} = 0.5632 P_{Sex} = 0.4067 P_{Int} = 0.0902
Labyrinth zone area (μm^2)	2209887.36 ± 23153.38	2560082.88 ± 210013.19	2292216.65 ± 148755.98	1966416.26 ± 188691.09	P_{Diet} = 0.1360 P_{Sex} = 0.9405 P_{Int} = 0.0563
Relative labyrinth zone area (% Total placental area)	37.832 ± 3.014	40.145 ± 1.319	40.770 ± 2.555	34.407 ± 2.196	P_{Diet} = 0.5632 P_{Sex} = 0.4067 P_{Int} = 0.0902
Total placental area (μm^2)	5972612.84 ± 550822.52	6372232.20 ± 475808.37	5624717.97 ± 154743.68	5692341.16 ± 237044.51	P_{Diet} = 0.2128 P_{Sex} = 0.5608 P_{Int} = 0.6783

CON, dams mated with CON males or pregnancies generated by CON males; PHF, dams mated with high fat diet-fed males or pregnancies generated by high fat diet-fed males. *Data are presented as mean ± SEM. Unpaired Student t test, Mann–Whitney test, or two-way ANOVA using Bonferonni post-hoc for multiple comparison. Groups that do not share the same letter indicate significance $P < 0.05$.

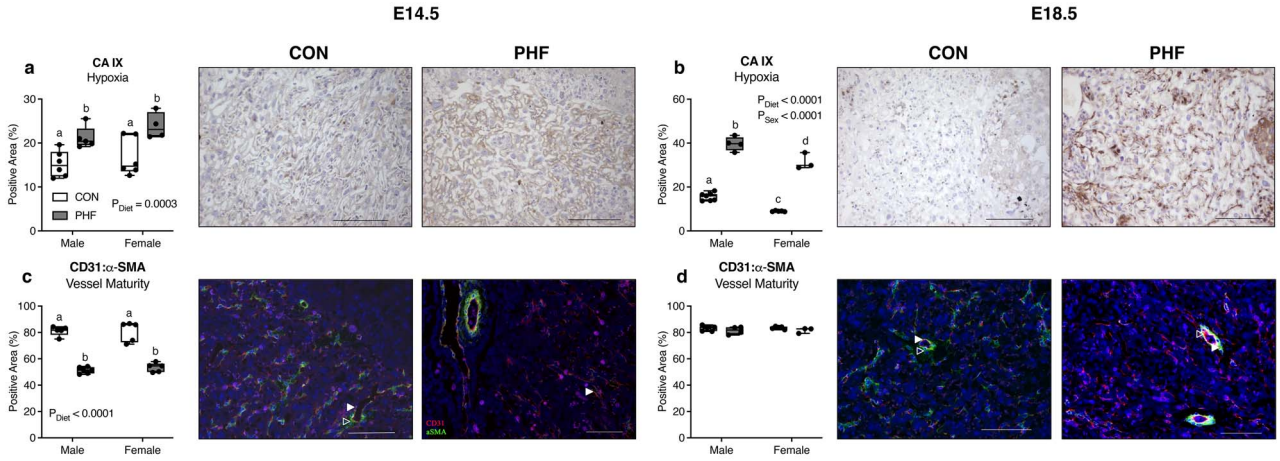

Figure 2. Paternal obesity results in hypoxic placentae and blood vessels with reduced integrity. Male and female CON and PHF placentae were immunostained for carbonic anhydrase 9 (CA IX, hypoxia marker), cluster of differentiation 31 (CD31, endothelial cell marker), and α-smooth muscle actin (α-SMA, pericyte marker). Box plots represent proportions (%) of immunopositive staining in whole placental sections. Representative images are from the labyrinth zone of female placentae. Magnification 20x, scale bars = 100 μm. (a) Percent immunopositive area of CA IX staining in E14.5 and (b) E18.5 placentae. (c) Ratio of CD31 (red, closed arrowhead) to α-SMA (green, open arrowhead) in E14.5 and (d) E18.5 placentae. CON; n = 5–7, PHF; n = 3–6. Data are presented as box and whisker plots; min to max with the center line representing the median. Two-way ANOVA with main effects of paternal diet and placental sex as factors. Box plots with different letters indicate significance $P < 0.05$ using Bonferroni's post-hoc for multiple comparison. CON = Control (open box plots); PHF = Paternal high fat diet-induced obesity (gray box plots).

area in tissue derived from CON and PHF males. CA IX immunostaining was increased in PHF placentae compared to CON ($P_{Diet} = 0.0003$) in male ($P = 0.0174$) and female ($P = 0.0077$; Figure 2A) placentae at E14.5, and this difference persisted to E18.5 ($P_{Diet} < 0.0001$, $P_{Sex} < 0.0001$) in PHF male ($P < 0.0001$) and female placentae ($P < 0.0001$; Figure 2B). Consistent with the presence of hypoxia, we also found increased protein levels of hypoxia-inducible factor 1-alpha (HIF-1α) in PHF placentae at E14.5 ($P_{Diet} = 0.0207$; Supplemental Figures S3A). HIF-1α protein levels were also greater in female placentae than male placentae at E18.5 ($P_{Sex} = 0.0208$; Supplemental Figures S3C).

As PHF placentae appeared hypoxic, we set out to determine whether paternal obesity impacted placental blood vessel structure. We measured the proportion of cells with positive immunostaining of pro-angiogenic factor VEGF-A, its receptor VEGFR-2, endothelial cell marker CD31, and pericyte marker α-SMA. Both human [31] and mouse [32] placenta are abundant in pericytes, which are perivascular cells that stabilize and regulate endothelial function. The ratio of CD31:α-SMA was decreased ($P_{Diet} < 0.0001$) in male and female PHF placentae ($P < 0.0001$; Figure 2C) compared to CON at E14.5, but similar between groups at E18.5 ($P_{Diet} = 0.0575$; Figure 2D; total placental area). Positive VEGF-A placental immunostaining was increased in male ($P_{Diet} < 0.0001$, $P < 0.0001$) and female PHF placentae ($P = 0.0002$; Figure 3A), although at E18.5 this difference persisted only in PHF female placentae ($P_{Int} = 0.0009$, $P_{Diet} = 0.0061$; $P = 0.0014$; Figure 3B). This is consistent with an increased VEGFR-2 immunostaining in PHF male ($P_{Diet} = 0.0002$, $P = 0.0209$) and female placentae ($P = 0.0029$; Figure 3C) at E14.5, and in female (but not male) PHF placentae at E18.5 ($P_{Diet} = 0.0015$, $P = 0.0096$; Figure 3D). These data suggest that placentae derived from PHF sires have increased angiogenesis but may result in vessels that lack pericyte integrity which might impact vessel function.

In keeping with this notion, we found reduced expression of transcription factors that mediate blood vessel development in PHF placentae. Heme oxygenase (HO, encoded by *Hmox1*) facilitates blood vessel development through regulating matrix metalloproteinases MMP14 and MMP2 [33]. Paternal obesity reduced transcript levels of *Hmox1* in male and female placentae at E14.5 ($P_{Diet} = 0.0203$), but not at E18.5 (Supplemental Table S6). *Mmp14* transcript levels were decreased in PHF female placentae at E14.5 ($P_{Diet} = 0.0014$, $P = 0.0152$), but these effects did not persist to E18.5 (Supplemental Table S6). *Mmp2* transcript levels were unchanged at E14.5 and at E18.5 (Supplemental Table S6). Therefore, it appears that paternal obesity may interfere with placental development by altering factors associated with blood vessel development and cellular matrix integrity.

Paternal obesity has little impact on ER stress proteins in the placenta

Since placental hypoxia induces angiogenic processes and placental ER stress [34, 35], we set out to determine whether disruptions in placental angiogenesis were associated with ER stress. We measured protein levels of the ER stress chaperone GRP78, as well as regulators and effectors of three branches of the UPR: ATF6, IRE1α, and PERK. Paternal obesity increased GRP78 protein levels in male (but not female) PHF placentae at E14.5 ($P_{Diet} = 0.0039$, $P = 0.0022$; Figure 4A and C) and at E18.5 ($P_{Sex} = 0.0247$, $P_{Int} = 0.0247$, $P = 0.0407$; Figure 4B and D), although these data were quite variable. Although *Atf6*, and *Edem1* transcript levels were similar between groups (Figure 4E–H), *Pdia2* levels were lower in E14.5 PHF female (but not male) placentae compared to CON ($P_{Diet} = 0.0139$, $P_{Int} = 0.0051$; $P = 0.0038$; Figure 4I), but not at E18.5 (Figure 4J).

The IRE1α arm of the UPR is ubiquitously expressed and elicits an adaptive response to ER stress, working to increase ER capacity and decrease ER load [36]. Paternal

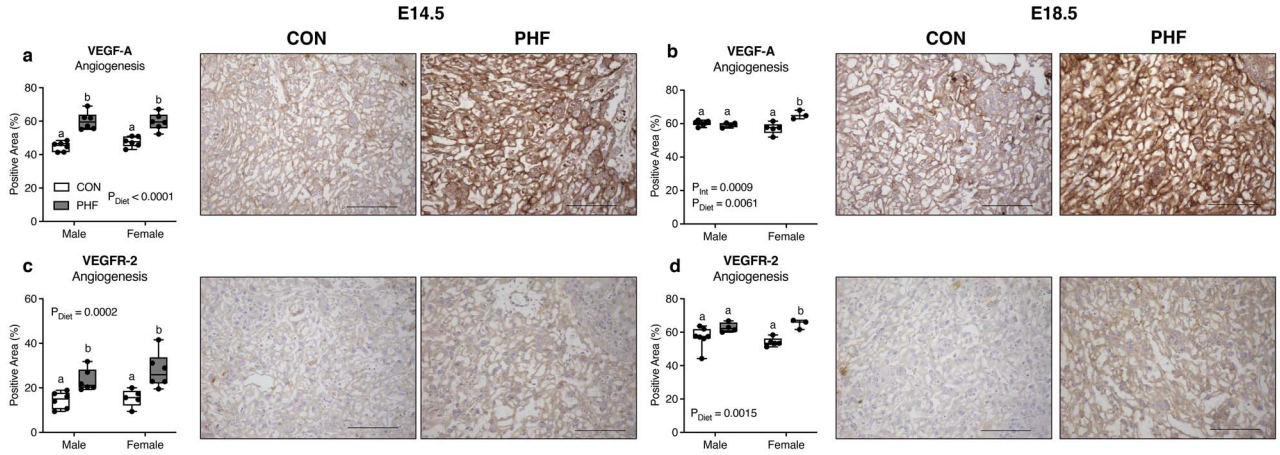

Figure 3. Paternal obesity alters angiogenic factors in the placenta. Male and female CON and PHF placentae were immunostained for vascular endothelial growth factor A (VEGF-A, proangiogenic factor), and vascular endothelial growth factor receptor 2 (VEGFR-2, proangiogenic factor). Box plots represent proportions (%) of immunopositive staining in whole placental sections; representative images are from the labyrinth zone of female placentae. Magnification 20x, scale bars = 100 μm. (a) Percent immunopositive area of VEGF-A staining in E14.5 and (b) E18.5 placentae. (c) Percent immunopositive area of VEGFR-2 staining in E14.5 and (d) E18.5 placentae. CON; $n = 5$–7, PHF; $n = 3$–6. Data are presented as box and whisker plots; min to max with the center line representing the median. Two-way ANOVA with main effects of paternal diet and placental sex as factors. Box plots with different letters indicate significance $P < 0.05$ using Bonferroni's post-hoc for multiple comparison. CON = Control (open box plots); PHF = Paternal high fat diet-induced obesity (gray box plots).

obesity had no impact on phosphorylated IRE1α at E14.5 although showed a significant interaction ($P_{Int} = 0.0488$; Supplemental Figure S5A and I). Levels were similar between groups at E18.5 (Supplemental Figure S5B and J). Levels of the downstream transcriptional target *Xbp1*, were similar between groups, including spliced (*Xbp1* (spliced)), total (*Xbp1* (total)), and the ratio of spliced *Xbp1* to total *Xbp1* (*Xbp1* (spliced): *Xbp1* (total); Supplemental Figure S5C,D,I,J, Table S7). We also investigated ER stress-activated proinflammatory signaling pathways that involve nuclear factor-B (NF-κB). At E14.5 and E18.5, NF-κB activity and transcript levels of inflammatory cytokines regulated by NF-κB, including *Traf6*, *Tnf* and *Il1b*, were similar between groups (Supplemental Table S7), although *Il6* transcript levels were moderately higher in PHF placental samples compared to CON (Supplemental Table S7).

The PERK arm of the UPR inhibits ribosomal function and globally diminishes protein production to accommodate protein stress adaptation [36]. Paternal obesity had a modest effect on the ratio of phosphorylated (phospho-) PERK to total PERK protein levels in E14.5 male (but not female) PHF placentae compared to CON, by an interaction only ($P_{Int} = 0.0018$, $P_{Sex} = 0.0010$; $P = 0.0356$; Supplemental Figure S5E). Similarly, phospho-PERK to total PERK protein levels were modestly increased in PHF placentae at E18.5 ($P_{Diet} = 0.0031$, $P = 0.0277$; Supplemental Figure S5F). Downstream of PERK activity, the phosphorylation of eukaryotic initiation factor 2A (eIF2α) promotes apoptosis, and the transcriptional activation of pro-apoptotic *Atf4* and *Ddit3* (the gene encoding CHOP) induce proteins involved in amino acid transport, autophagy, folding chaperones, redox regulatory proteins, and pro-apoptotic molecules [36]. The ratio of phospho-eIF2α to total eIF2α protein levels and transcript levels of *Atf4* and *Ddit3* were unchanged with PHF (Supplemental Table S8, Supplemental Figure S4). Pro-apoptotic *Bax* transcript levels were unchanged in PHF placentae at E14.5 and E18.5 (Supplemental Table S8); however, anti-apoptotic *Bcl2* transcript levels were increased in female (but not male) PHF placentae at E18.5 ($P_{Diet} = 0.0253$, $P = 0.0312$) but not E14.5 (Supplemental Table S8). The ratio of *Bax* to *Bcl2* transcripts levels was unchanged at E14.5 (Supplemental Figure S5G); however, at E18.5, the ratio of *Bax* to *Bcl2* transcript levels was significantly reduced in PHF female placentae ($P_{Int} = 0.0380$, $P_{Diet} = 0.0014$, $P = 0.0031$, Supplemental Figure S5H). Collectively, our data suggest that while paternal obesity may modestly increase PERK and IRE1α in total PHF placental homogenates, there is no significant impact on downstream signaling pathways through either the PERK or IRE1α branches, or that apoptosis markers are altered in PHF placenta at E14.5 or E18.5. However, future studies are warranted to investigate whether paternal obesity induces ER stress in specific placental components (i.e. junctional zone versus labyrinth zone).

Paternal obesity alters placental amino acid system A nutrient transporter expression

Since we observed changes with PHF indicative of placental hypoxia and altered vessel integrity, we next investigated whether placental nutrient transporter expression was impacted by PHF. Transcript levels of *Slc38a2*, which encodes sodium-coupled neutral amino acid protein 2 (SNAT2), were similar between groups at E14.5 (Supplemental Table S9) but were higher in female PHF placentae compared to CON at E18.5 ($P_{Int} = 0.0282$, $P_{Diet} = 0.0837$; $P = 0.0493$; Supplemental Table S9). In contrast, transcript levels of genes that encode glucose transporter 1 (GLUT1, *Slc2a1*) and GLUT3 (*Slc2a3*) were similar between groups (Supplemental Table S9), as were transcript levels of *Fabp4*, which encodes fatty acid binding protein (Supplemental Table S9). These data suggest that paternal obesity may change amino acid transport in late gestation but does not appreciably impact the expression levels of other placental nutrient transporters.

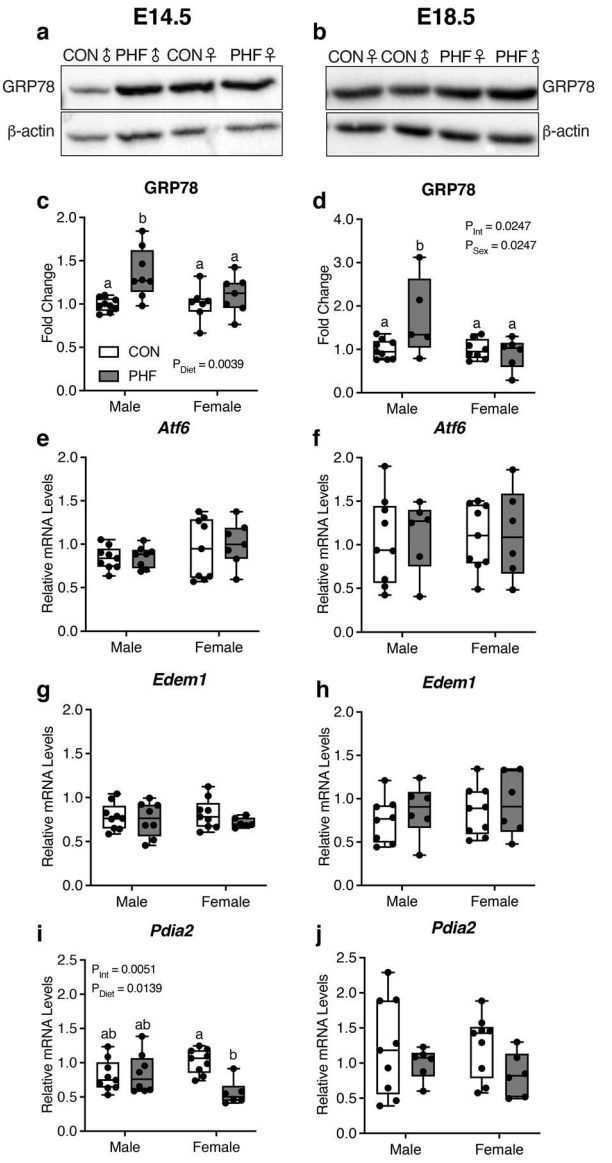

Figure 4. Paternal obesity has modest effects on the UPR in E14.5 and E18.5 placentae. GRP78 protein levels were semi-quantified using Western blotting in CON and PHF E14.5 and E18.5 whole placental homogenates. All data were normalized to loading control β-actin. Transcript levels of *Atf6* pathway and downstream targets were quantified using RT-qPCR in CON and PHF E14.5 and E18.5 whole placental homogenates. (a) Representative Western blot bands for GRP78 protein and loading control β-actin in male and female CON and PHF E14.5 and (b) E18.5 placentae. (c) GRP78 protein levels in E14.5 and (d) E18.5 placentae. (e) *Atf6* transcript levels in E14.5 and (f) E18.5 placentae. (g) *Edem1* transcript levels in E14.5 and (h) E18.5 placentae. (i) *Pdia2* transcript levels in E14.5 and (j) E18.5 placentae. CON; $n = 7$–9, PHF; $n = 5$–8. Data are presented as box and whisker plots; min to max with the center line representing the median. Two-way ANOVA with main effects of paternal diet and placental sex as factors. Box plots with different letters indicate significance $P < 0.05$ using Bonferroni's post-hoc for multiple comparison. CON = Control (open box plots); PHF = Paternal high fat diet-induced obesity (gray box plots).

Paternal obesity alters placental IGF2 and IRS transcripts at mid-gestation

Insulin-like growth factor 2 (*Igf2*) is paternally imprinted. In human studies, paternal obesity is associated with newborn hypomethylation of insulin-like growth factor 2 (IGF2) protein and ER stress altered this IGF2 bioactivity [37]. Transcript levels of *Igf2* were elevated in PHF placentae at E14.5 ($P_{Diet} = 0.0002$, $P = 0.0009$; Figure 5A), particularly in females. This increase did not persist to E18.5 (Figure 5D). IGF2 binds to IGF-1R, IGF-2R, and insulin receptors (IR) [38] and targets insulin receptor substrate 1 (IRS1) and IRS2, to promote placental growth and development through cell proliferation, survival, and mitogenesis [39]. Consistent with increased *Igf2* levels, *Irs1* transcripts were elevated in PHF placentae at E14.5 ($P_{Diet} = 0.0483$, $P_{Sex} = 0.0041$; Figure 5B) but were similar between groups at E18.5 (Figure 5E). Transcript levels of *Irs2* were similar between groups at E14.5 (Figure 5C). At E18.5 transcript levels were affected by paternal diet and placental sex ($P_{Int} = 0.0068$; Figure 5F).

Paternal obesity does not impact maternal metabolic adaptation to pregnancy

Since maternal adaptations to pregnancy directly impact the intrauterine environment and thus fetal development, we next investigated whether paternal obesity *indirectly* modified the *in utero* milieu via changes to maternal glucose metabolism. The placenta secretes endocrine factors, including placental lactogen (PL), which facilitate maternal metabolic adaptations to pregnancy [40]. Since we observed significant changes in placental development in pregnancies sired by PHF, we investigated whether paternally induced placental-mediated changes in maternal glucose tolerance were impacted. We observed that at both time points in pregnancy, maternal glucose tolerance is unaltered by PHF (Figure 5G–J). Transcript levels of placental lactogen I coding-gene (*Prl3d1)* were unaltered at E14.5 (Figure 5K) by PHF, although at E18.5 levels were lower in female compared to male placentae ($P_{Sex} = 0.0021$; $P = 0.0140$; Figure 5M). Expression levels of *Prl3b1* were similar between groups at E14.5 (Figure 5L) and E18.5 (Figure 5N). Histological analyses of parietal trophoblast giant cell number, one of the cell types that produce PL (Figure 5O–Q), were unchanged. Our findings suggest that maternal glucose tolerance, as well as placental capacity to produce PL, was unaffected by obesity in the father.

Paternal obesity alters factors that regulate fetal hepatic gluconeogenesis

Paternal obesity is associated with glucose intolerance in adult offspring, particularly in females [36]. Since fetal hepatic gluconeogenesis contributes to postnatal glucose tolerance, and maternal obesity is associated with changes in fetal gluconeogenic enzyme expression [5], we investigated whether paternal obesity similarly impacts fetal metabolic development. Hepatocyte nuclear factors (HNFs) play an important role in embryonic hepatic development. HNF4A is a key regulator of many genes involved in hepatic function, and its targeted deletion in the liver results in steatosis and severe disruption of gluconeogenesis [41]. Although transcript levels of *Hnf4a* were unaltered at E14.5, levels were higher in PHF male (but not female) livers compared to CON at E18.5 ($P_{Int} = 0.0229$, $P_{Sex} = 0.0008$, $P_{Diet} < 0.0001$; $P = 0.0001$; Supplemental Figure S6A and B). Transcript levels of the HNF4A co-activator, peroxisome proliferative activated receptor gamma coactivator 1-alpha (*Ppargc1α*), were also similar between groups at E14.5, but increased at E18.5, albeit only in female PHF livers ($P_{Diet} = 0.0213$, $P = 0.0334$;

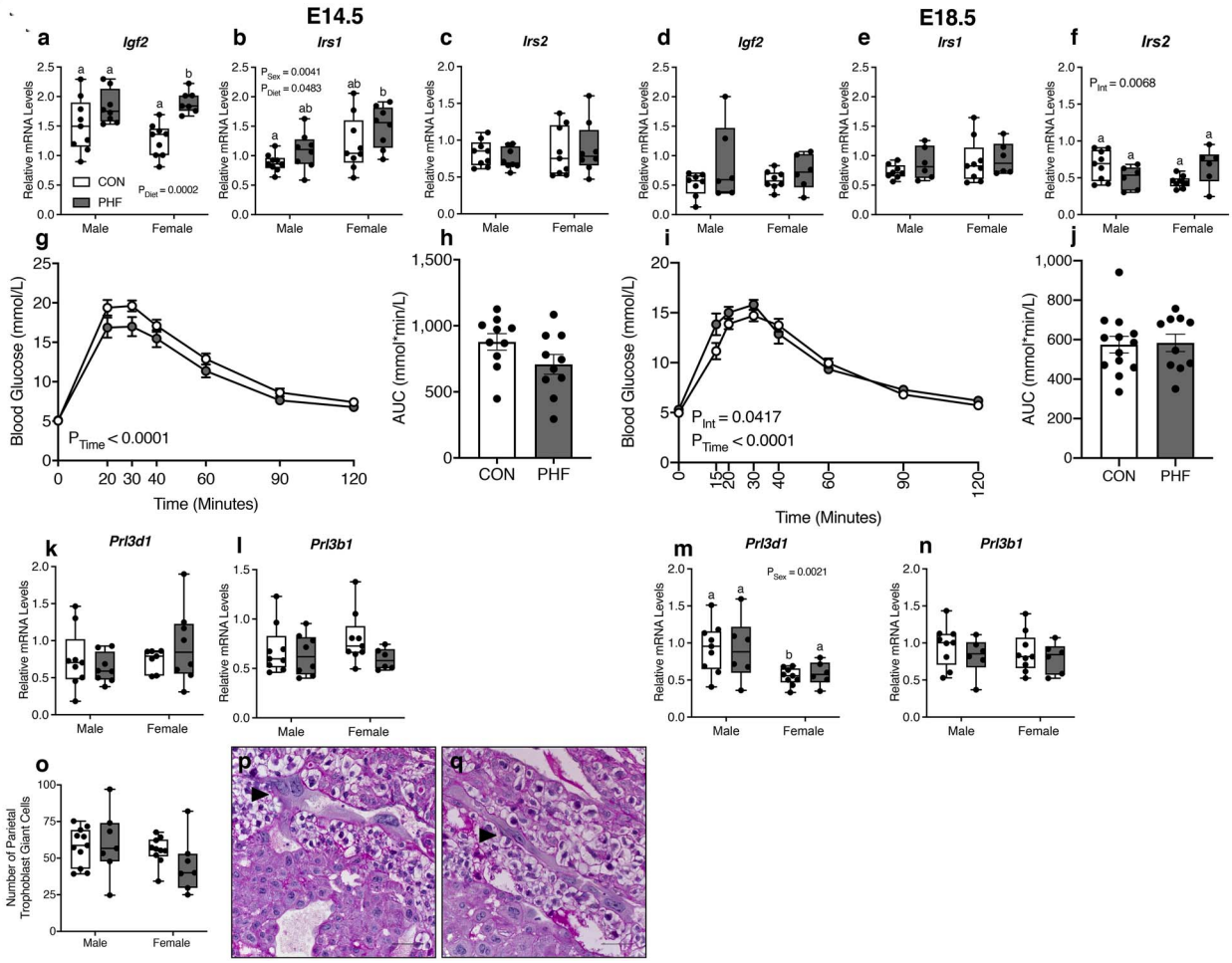

Figure 5. Paternal obesity alters placental *Igf2, Irs1, and Irs2* transcripts in a sex-specific manner but does not impact maternal glucose tolerance or placental lactogen. (a) Transcript levels of *Igf2*, (b) *Irs1*, and (c) *Irs2* in E14.5 placentae. (d) Transcript levels of *Igf2*, (e) *Irs1*, and (f) *Irs2* in E18.5 placentae. (g) Maternal glucose tolerance, and (h) glucose area under the curve (AUC) at E14.5. (i) Maternal glucose tolerance, and (j) glucose AUC at E18.5. (k) *Prl3d1* transcript levels at E14.5 and at (l) E18.5. (m) *Prl3b1* transcript levels at E14.5 and at (n) E18.5. (o) Number of parietal trophoblast giant cells in CON and PHF placentae. (p) Representative photos of E14.5 CON and (q) PHF placental samples stained for glycogen using PAS. Arrowheads show placental parietal trophoblast giant cells. Magnification 20x, scale bars = 50 μm. CON; $n = 7$–13, PHF; $n = 6$–10. Data are presented as mean ± SEM for glucose tolerance, and as box and whisker plots; min to max with the center line representing the median for transcript levels. Glucose tolerance was measured using two-way repeated measures ANOVA or mixed-effects model with main effects of paternal diet and time as factors using Bonferroni post-hoc for multiple comparison; or by unpaired Student *t*-test. Placental transcripts were measured using two-way ANOVA with main effects of paternal diet and placental sex as factors. Box plots with different letters indicate significance $P < 0.05$ using Bonferroni post-hoc for multiple comparison. CON = Control (open circles and box plots); PHF = Paternal high fat diet-induced obesity (gray circles and box plots).

Supplemental Figure S6C and D). Transcript levels of hepatic glucose-6-phosphatase (*G6pc*), which hydrolyzes glucose-6-phosphate and frees glucose, were higher in females compared to males at E14.5 ($P_{Sex} = 0.0216$), but PHF did not affect *G6pc* levels at E18.5 (Supplemental Figure S6E and F). Levels of the rate-limiting enzyme in gluconeogenesis, phosphoenolpyruvate carboxykinase 1 (*Pck1*), were similar between groups (Supplemental Figure S6G and H). These results suggest that expression of hepatic gluconeogenic transcriptional activators is increased in PHF fetuses at E18.5, but expression of key downstream gluconeogenic enzymes is unaffected.

Paternal obesity has modest impacts on ER stress proteins in the fetal liver

Maternal obesity has been associated with ER stress in offspring [42]. We investigated whether paternal obesity similarly impacts ER stress-induced effectors, but extended investigations to much earlier in development. Transcript levels of *Hspa5*, the gene that encodes for ER stress chaperone GRP78, were increased in female PHF livers compared to CON at E14.5 ($P_{Diet} = 0.0013$, $P = 0.0202$; Figure 6A). GRP78 protein levels however, were unchanged at E18.5 (CON male; 1.000 ± 0.167, CON female; 1.000 ± 0.109, PHF male; 0.919 ± 0.075, PHF female; 1.531 ± 0.449). Hepatic expression of *Eif2ak3*, the gene that encodes for PERK, was increased in PHF fetuses at E14.5 (CON male; 1.162 ± 0.189, CON female; 1.118 ± 0.219, PHF male; 1.930 ± 0.215, PHF female; 1.533 ± 0.366; $P_{Diet} = 0.0333$). Due to lack of sufficient sample, we were unable to measure transcript levels of *Eif2ak3* at E18.5. However, protein levels of fetal hepatic phospho-PERK at E18.5 were increased in male PHF fetuses but not females ($P_{Diet} = 0.0018$; $P = 0.0127$; Figure 6B). Activation of the PERK arm of the UPR was associated with increased transcript levels of pro-apoptotic factor, *Ddit3*, the CHOP-encoding gene, in fetal PHF livers at E14.5 ($P_{Diet} = 0.0075$, $P = 0.0234$; Figure 6C) and in fetal

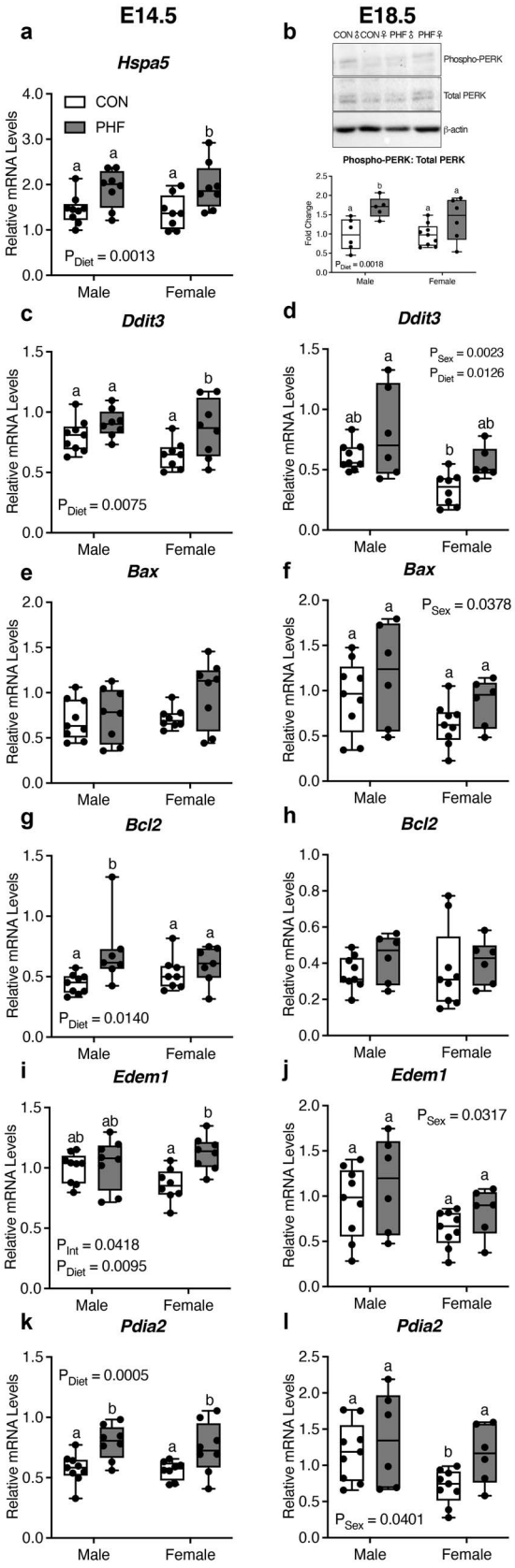

Figure 6. Paternal obesity activates the unfolded protein response in fetal liver. Transcript levels of *Hspa5*, PERK, and apoptosis-related genes were quantified using RT-qPCR in CON and PHF E14.5 and/or E18.5 liver. Ratio of protein levels of phospho-PERK:total PERK were semi-quantified using Western blotting in CON and PHF E18.5 liver. Total PERK protein levels were normalized to β-actin. (a) *Hspa5* transcript levels in E14.5 liver. (b) Representative Western blot bands and densitometry data for Phospho-PERK: Total PERK protein levels and loading control β-actin in male and female CON and PHF E18.5 liver. (c) *Ddit3* transcript levels in E14.5 and (d) E18.5 liver. (e) *Bax* transcript levels in E14.5 and (f) E18.5 liver. (g) *Bcl2* transcript levels in E14.5 and (h) E18.5 liver. (i) *Edem1* transcript levels in E14.5 and (j) E18.5 liver. (k) *Pdia2* transcript levels in E14.5 and (l) E18.5 liver. CON; $n = 6$–9, PHF; $n = 5$–8. Data are presented as box and whisker plots min to max; with the center line representing the median. Two-way ANOVA with main effects of paternal diet and fetal sex as factors. Box plots with different letters indicate significance $P < 0.05$ using Bonferroni's post-hoc for multiple comparison. CON = Control (open box plots); PHF = Paternal high fat diet-induced obesity (gray box plots).

PHF livers at E18.5 ($P_{Diet} = 0.0126$, $P_{Sex} = 0.0023$; Figure 6D), suggesting that the process of apoptosis may be elevated in PHF fetal livers. Consistent with this, protein levels of cleaved caspase 3 were also increased in PHF livers in E18.5 (CON male; 1.051 ± 0.119, CON female; 1.003 ± 0.090, PHF male; 1.811 ± 0.643, PHF female; 1.595 ± 0.402; $P_{Diet} = 0.0347$, Supplemental Figure S4). Transcript levels of *Bax* were unchanged at E14.5 (Figure 6E) and decreased in females at E18.5 ($P_{Sex} = 0.0378$; Figure 6F). Expression of *Bcl2* was increased in PHF male livers compared to CON male livers ($P_{Diet} = 0.0140$, $P = 0.0120$; Figure 6G) at E14.5, but these changes did not persist to E18.5 (Figure 6H). The ratio of *Bax* to *Bcl2* transcript levels were unchanged (Supplemental Table S10). These data suggest that further investigation into the balance of fetal hepatic apoptosis and proliferation is required. Matched protein levels of ER stress markers coupled with histological sections of markers of proliferation (Ki67) and apoptosis could elucidate whether PHF alters fetal hepatic development.

The native ER protein, ATF6, controls one of the three branches of the UPR and has been shown to be assisted by EDEM1. ATF6 is selectively translated by the phosphorylation of eIF2α and participates in a feedback loop by inducing expression of eIF2α phosphatase, GADD34 [43]. Transcript levels of *Atf6* were increased in PHF livers at E14.5, but not at E18.5 (Supplemental Table S10). *Ppp1r15a*, the gene that encodes for GADD34, was similar between groups at E14.5 and E18.5 (Supplemental Table S10). Transcript levels of *Edem1* were higher in female PHF compared to female CON liver at E14.5 ($P_{Int} = 0.0418$, $P_{Diet} = 0.0095$, $P = 0.0112$; Figure 6I) but not at E18.5. In general, *Edem1* transcripts were lower in female compared to male livers at E18.5 ($P_{Sex} = 0.0317$; Figure 6J). In addition to the main branches of the UPR, there are many genes that have crucial functions in protein folding that are altered with ER stress. PDIA2 is responsible for protein folding and thiol-disulfide exchanges and is mediated by transcription factor AFT6 [44]. Transcript levels of *Pdia2* were increased in PHF ($P_{Diet} = 0.0005$) male ($P = 0.0094$; Figure 6K) and female ($P = 0.0366$; Figure 6K) livers at E14.5, but at E18.5, *Pdia2* expression levels were decreased in female CON liver compared to male CON liver ($P_{Sex} = 0.0401$, $P = 0.0477$; Figure 6L).

Finally, we investigated whether the IRE1 branch of the UPR was altered in PHF fetal livers. Neither IRE1α transcript nor protein levels were altered in CON and PHF E14.5 and E18.5 liver; the ratio of spliced *Xbp1* to total *Xbp1* was similar between groups (Supplemental Table S10). Thus, although it appears that the PERK and ATF6 arms of the UPR

may be altered in fetal liver in response to paternal obesity, the IRE1 branch is not.

Paternal obesity impacts offspring whole body energetics and glucose tolerance

Paternal obesity significantly impacts offspring metabolism [7]. CON and PHF male and female offspring gained similar amounts of weight (Supplemental Figure S7A and B). Despite this, offspring gonadal fat mass was affected by both offspring sex and paternal diet ($P_{Sex} < 0.0001$, $P_{Int} = 0.0153$; Supplemental Figure S7C); whereas PHF male offspring had lower fat mass, PHF females had higher fat mass. Although paternal obesity did not affect liver weight, overall females had lighter livers compared to males ($P_{Sex} < 0.0001$, $P = 0.0007$; Supplemental Figure S7D).

We also investigated whether paternal obesity alters whole body energy metabolism in offspring. Using a sophisticated metabolic assessment system of indirect calorimetry [45], we calculated whether paternal obesity changed the type and rate of substrate utilization by offspring, while also measuring 48-h activity and food consumption light and dark cycles for 24 h. Food consumption was higher in PHF female and male offspring ($P_{Diet} = 0.011$; Figure 7A) and was especially higher during the dark compared to light cycle of the day. Heat production, a marker of overall energy consumption, tended to be lower in PHF offspring ($P_{Diet} = 0.055$; Figure 7B) and greater in female offspring. Total activity was lower in male ($P_{Sex} = 0.041$; Figure 7C) compared to females overall and tended to be even lower in PHF females compared to CON—particularly during the light cycle. Oxygen consumption ($VO_2 = O_2$ inhaled per unit time) was lower in male PHF offspring ($P_{Sex} < 0.0001$; Figure 7D), as was CO_2 production ($VCO_2 = CO_2$ exhaled from the body per unit time; $P_{Sex} = 0.004$; Figure 7E), and tended to be lower in females—again especially during the light cycle.

Using VO_2 and VCO_2 we calculated the RER to estimate the respiratory quotient (RQ), an indicator of which fuel (e.g. carbohydrate or fat) is being metabolized [45]. An RER value near 0.7 suggests that fat is the predominant fuel source, a RER value near 1.0 suggests that carbohydrate is the predominant fuel source, and a RER value between 0.7 and 1.0 suggests a combination of fat and carbohydrate is being used. Although RER tended to be lower in PHF offspring during the light cycle, this difference was not statistically significant (Figure 7F), although lipid oxidation was lower in male offspring ($P_{Sex} = 0.012$; Figure 7G). These data suggest that basal metabolic rate appears moderately lower in PHF offspring and impacts of paternal obesity on whole body energy metabolism in offspring is sex-specific [7].

Consistent with other work, paternal obesity increased fasting blood glucose levels in male and female offspring at P60 (CON male; 8.7 ± 0.2, CON female; 7.6 ± 0.1, PHF male; 9.5 ± 0.2, PHF female; 8.1 ± 0.3, $P_{Diet} = 0.017$, $P_{Sex} < 0.0001$). Paternal obesity impaired glucose tolerance in both female ($P_{Diet} < 0.0001$; Figure 7H) and male ($P_{Diet} = 0.0042$; Figure 7I) offspring. Thus, paternal obesity is associated with changes in both whole body metabolism and glucose intolerance in young adult offspring.

Discussion

Although the first experimental data showing that paternal diet/obesity impaired offspring glucose tolerance were published over a decade ago [7], we still know very little of the mechanisms underpinning this relationship. We show that paternal obesity alters markers suggestive of placental hypoxia, altered placental angiogenesis, and blood vessel integrity. Placentae associated with a female fetus are especially vulnerable, showing changes to transcription factors that regulate placental vascular remodeling, as well as increased placental *Igf2*, and increased expression of amino acid transporter SNAT2. Paternal obesity significantly impacts the fetus, possibly activating hepatic ER stress through PERK and ATF6 arms of the UPR, which may have downstream impacts on gluconeogenesis. These changes, however, are not the result of modifications to maternal metabolic adaptation to pregnancy, since we show that paternal obesity does not affect maternal glucose metabolism or the number of parietal trophoblast giant cells that contribute to PL production. Thus, we believe that paternal obesity impacts fetal metabolic signaling pathways and offspring glucose intolerance and whole-body energetics via impairments in placental vasculature and possibly reducing in utero oxygenation. Overall, our data suggest that intrauterine changes in placental function may drive changes in fetal hepatic development which could underpin metabolic dysfunction in male and female offspring, and changes in offspring metabolic rate.

Placental increases in hypoxia markers HIF-1α and CA IX, pro-angiogenic markers VEGF and VEGFR-2, and decreases in the vessel integrity marker CD31:α-SMA ratio at E14.5 suggests that paternal obesity induces placental hypoxia through pro-angiogenic pathways and may impair pericyte development and blood vessel stability at mid-gestation. Our data are consistent with the hypothesis that hypoxia can activate a sequence of events starting with upregulation of HIF-1α production [46]. As the increase in HIF-1α and reduction in CD31:α-SMA ratio were observed in PHF placentae at E14.5, but not at E18.5, we hypothesize that vessel compromise may be a result of the timing of angiogenesis being perturbed by PHF. Angiogenesis begins in the murine placenta after E8.5 [47], thus it is possible that early impairments manifest as hypoxia and reduced vessel integrity at E14.5, which is resolves by E18.5. Future studies further investigating whether paternal obesity delays placental blood vessel development are warranted.

Experimental studies in mice have shown that maternal obesity induces placental ER stress and impairs placental vascularization [4, 5]. ER stress promotes VEGF expression [48] through enhanced phosphorylation of HIF-1α [49]. Our data suggest the impact of paternal obesity on placental angiogenesis is not driven by ER stress, markers of which were only modestly increased in whole placental homogenate. An alternative hypothesis may be a reduced rate of arterial oxygen delivery to the placenta and/or an increase in oxygen consumption/requirement in PHF placenta. No data exist describing the impacts of paternal obesity on either placental blood flow or oxygen consumption, but future work should investigate whether reduced oxygen delivery via maternal arteries or increased placental oxygen consumption underpin the observed hypoxia in PHF placentae. Interestingly, data exist in humans to suggest that fetal sex impacts maternal vascular adaptation to pregnancy [50] and highlight the need to investigate whether sex-specific alterations occur in placental blood flow and/or placental oxygen delivery in pregnancies of high fat-fed fathers.

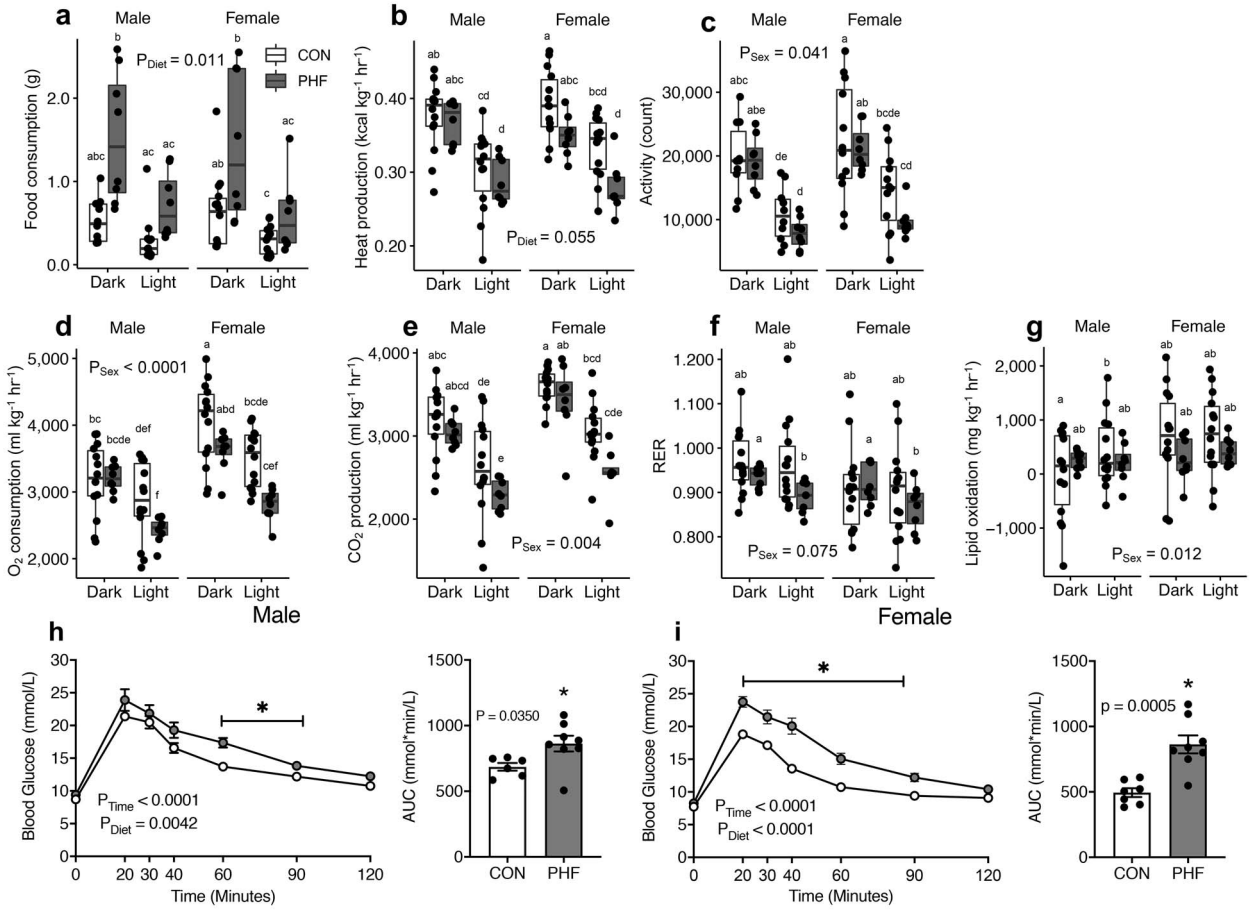

Figure 7. Paternal obesity alters whole body energy metabolism and induces glucose intolerance in offspring. Young adult CON and PHF male and female offspring were subjected to *in vivo* metabolic assessment at P53 and a glucose tolerance test at P60. (a) Adult CON and PHF male and female offspring food consumption, (b) heat production, (c) total horizontal motor activity, (d) oxygen consumption, (e) carbon dioxide production, (f) respiratory exchange ratio, and (g) lipid oxidation. (h) Adult CON and PHF glucose tolerance and glucose AUC in male, and (i) female offspring. Metabolic assessments data are presented as box and whisker plots; min to max with the center line representing the median. Glucose tolerance test and AUC are presented as mean ± SEM. CON; $n = 6–7$, PHF; $n = 5–8$. Two-way repeated measures ANOVA with main effects of paternal diet and time as factors using Bonferroni post-hoc for multiple comparison or Student *t*-test. Metabolic assessments presented as box plots with different letters denote $P < 0.05$ in a linear mixed-effects model with main effects and multiple comparisons determined by Satterthwaite's method of approximation. CON = Control (open circles and box plots); PHF = Paternal high fat diet-induced obesity (gray circles and box plots).

This is of particular relevance since many of our outcomes appear to be predominant in female placenta and offspring. In human pregnancy, female fetal sex is associated with increased risk for early preterm preeclampsia, one of the pregnancy complications associated with placental hypoxia [35], in association with proinflammatory cytokines in the first trimester [51, 52]. Our finding that female placentae are particularly impacted by PHF is consistent with these observations in humans preeclamptic placentae [53]. We have previously reported that maternal obesity results in placental inflammation at mid-gestation [5]. Whether proinflammatory cytokines are involved in sex-specific changes in PHF placentae is beyond the objectives of the current study, although we show some evidence of an increase in IL6 transcript levels in PHF placentae at term gestation. We also found sex-specific impacts of PHF on the placental nutrient transporter *Slc38a2* (SNAT2), which was increased in females E18.5. SNAT2 transports neutral amino acids, including gluconeogenic substrates alanine and glutamine [54, 55]. SNAT2 expression is induced by hypoxia in *in vitro* and *in vivo* in cancer models [56] and may be similarly induced by hypoxia in PHF placentae, although further experiments are required to test this hypothesis. It may be that an increase in placental transfer of gluconeogenic amino acids in PHF pregnancies, contributes to changes in fetal hepatic gluconeogenic signaling molecules at E18.5.

Placental growth is regulated by IGFs [57]. We show increased *Igf2* transcript levels in PHF placentae, consistent with increased levels of *Irs1*. IGFs have both proliferative and anti-apoptotic effects on trophoblasts [58]. IGF2 may also be activating downstream signaling pathways through IRs. In placental arterial endothelial cells, activation of IR induces endothelial nitric oxide synthase (eNOS), which has been proposed to facilitate angiogenesis through HIF-1α, VEGF, and VEGFR-2 [59]. Indeed, in mice, IGF2 increases labyrinth zone volume and surface area dedicated to transport [60]. If this is happening in our model, increased surface area may protect against the negative impacts of hypoxia on fetal growth, which would explain the similar fetal and placental weights of PHF and controls.

Prenatal stressors, including improper nutrition or hypoxia, induce fetal adaptations in metabolic organs including the liver. Maternal obesity in mice, results in ER stress in offspring liver [61]. Although paternal obesity leads to impaired glucose tolerance and liver steatosis in murine offspring [62], few studies have investigated whether changes in the fetal liver contribute to offspring metabolic dysfunction. We observed increased transcript levels of key markers of the UPR in PHF fetal livers. These increases were accompanied by elevated levels of cleaved caspase-3, suggesting paternal obesity may increase fetal hepatic apoptosis. As hepatic ER stress is associated with changes in hepatic glucose metabolism, we investigated transcriptional regulators of gluconeogenesis. Paternal obesity modestly increased fetal hepatic transcript levels of pro-gluconeogenic factor *Ppargclα* and its co-regulator *Hnf4a* [63] at term gestation, although we did not test whether these changes in *Ppargclα* and *Hnf4a* persist postnatally. As previously discussed, it is possible that these fetal hepatic changes are downstream of increases in gluconeogenic substrates; where PHF results in poor placental oxygenation and increased SNAT2 activity and placental transfer of gluconeogenic amino acids. This hypothesis however needs to be tested in future studies.

We propose that impacts of PHF on the fetal liver are evident postnatally. We show that paternal obesity induces offspring glucose intolerance but also impairs whole body energy utilization and metabolism. Previous work suggests that *in utero* adversity activates the hepatic UPR, increases expression of gluconeogenic genes in pups, and results in glucose intolerance in male offspring [64]. No data exist describing the impacts of paternal obesity on offspring basal metabolic rate. We show alterations in whole body energetics, including physical activity, heat production, and O_2 and CO_2 dynamics in PHF offspring. Offspring of obese fathers were glucose intolerant, ate more, and moved less throughout the day, which may contribute to or be a function of a reduction in their basal metabolic rate. This appeared more prevalent in female offspring, particularly during the light cycle of the day. Our data contribute to early work showing that female, but not male, offspring born to high fat-fed fathers have impaired glucose tolerance and insulin deficiency [7] and extend these data showing that young female offspring have higher fat mass, and reduced activity and basal metabolism as early as ~60 days of age. Although it is unknown what underlying mechanisms are responsible for these changes to metabolism, our data suggest that an adverse hypoxic intrauterine environment, particularly in females, which appears to include impaired placental vessel development, may fuel changes to whole body energetics and could fuel long-term development of obesity and result in insulin resistance.

We recognize that our study has limitations. We performed a global investigation of paternal obesity on placental markers of hypoxia, ER stress, and nutrient transport using whole placental homogenate. Future studies should investigate junctional and labyrinth zones of placentae to assess markers of interest in specific placental regions. Additionally, we did not perform placental stereology to determine whether the vascular changes we observe also impact maternal–fetal surface exchange. It is unknown whether the placental hypoxia that we observe is a result of reduced arterial oxygen delivery to the placenta or increased oxygen consumption. Subsequent studies investigating the source of placental hypoxia are necessary. Although we observe some evidence of potential fetal hepatic ER stress, experiments that specifically investigate the UPR signaling and ER stress (potentially using transgenic mice or pharmacological agents) in both fetuses and offspring should be conducted. Finally, we do not know whether placental hypoxia results in fetal hypoxia, which could be a driver of hepatic ER stress; these studies are now warranted.

In conclusion, paternal obesity-induced glucose intolerance and metabolic dysfunction in offspring appears driven by impaired placental vascular development and placental hypoxia. We postulate that impaired placental function results in an adverse intrauterine environment that could promote ER stress-mediated adaptations in fetal hepatic development, predisposing offspring to postnatal impaired energetics and metabolic compromise.

Authors' contributions

P.A.J. wrote the manuscript. P.A.J., V.S.P., and T.A.R conducted the animal work, data collection, and data analysis. E.Y. conducted molecular analyses in E18.5 fetal livers. K.M.K. analyzed offspring CLAMS data. J.J.P. conducted IHC experiments in E14.5 and E18.5 placentae. P.A.J., V.S.P., T.A.R., and D.M.S. interpreted the data. D.M.S. designed the experiments and wrote the manuscript. All authors have reviewed and approved the final manuscript.

Acknowledgments

We thank the CNPq Science without Boarders Exchange Program that funded Dr Ribeiro's exchange with the Sloboda Lab during the time of data collection. We would like to thank Dr Gregory R. Steinberg (Department of Medicine, McMaster University) for use of the body composition analyzer and CLAMS, and Drs Rebecca J. Ford and James S. Lally (Department of Medicine, McMaster University) for their assistance with CLAMS analysis. We thank Mr Andrew De Jong for his assistance with immunoblotting experiments in fetal liver. This work was funded by the Natural Sciences and Engineering Research Council of Canada.

Supplementary material

Supplementary material is available at *BIOLRE* online.

Data availability

Offspring CLAMS data available at https://github.com/kennek6/PaternalHFD_CLAMS.

Conflict of interest

The author(s) declare no potential conflict of interest with respect to research, authorship, and/or publication of this article.

References

1. World Health Organization Fact sheets. *Obesity and Overweight*. World Health Organization; 2020. https://www.who.int/news-room/fact-sheets/detail/obesity-and-overweight.
2. Fleming TP, Watkins AJ, Velazquez MA, Mathers JC, Prentice AM, Stephenson J, Barker M, Saffery R, Yajnik CS, Eckert JJ, Hanson MA, Forrester T *et al.* Origins of lifetime health around the time of conception: causes and consequences. *The Lancet* 2018; **391**: 1842–1852.
3. Lane M, Robker RL, Robertson SA. Parenting from before conception. *Science* 2014; **345**:756–760.

4. Gohir W, Kennedy KM, Wallace JG, Saoi M, Bellissimo CJ, Britz-McKibbin P, Petrik JJ, Surette MG, Sloboda DM. High-fat diet intake modulates maternal intestinal adaptations to pregnancy and results in placental hypoxia, as well as altered fetal gut barrier proteins and immune markers. *J Physiol* 2019; **597**:3029–3051.
5. Wallace JG, Bellissimo CJ, Yeo E, Fei Xia Y, Petrik JJ, Surette MG, Bowdish DM, Sloboda DM. Obesity during pregnancy results in maternal intestinal inflammation, placental hypoxia, and alters fetal glucose metabolism at mid-gestation. *Sci Rep* 2019; **9**:17621.
6. Danielzik S, Langnase K, Mast M, Spethmann C, Muller MJ. Impact of parental BMI on the manifestation of overweight 5-7 year old children. *Eur J Nutr* 2002; **41**:132–138.
7. Ng SF, Lin RC, Laybutt DR, Barres R, Owens JA, Morris MJ. Chronic high-fat diet in fathers programs beta-cell dysfunction in female rat offspring. *Nature* 2010; **467**:963–966.
8. Fullston T, Teague EMCO, Palmer NO, DeBlasio MJ, Mitchell M, Corbett M, Print CG, Owens JA, Lane M. Paternal obesity initiates metabolic disturbances in two generations of mice with incomplete penetrance to the F2 generation and alters the transcriptional profile of testis and sperm microRNA content. *FASEB J* 2013; **27**: 4226–4243.
9. Binder NK, Hannan NJ, Gardner DK. Paternal diet-induced obesity retards early mouse embryo development, mitochondrial activity and pregnancy health. *PLoS One* 2012; **7**:e52304.
10. Binder NK, Mitchell M, Gardner DK. Parental diet-induced obesity leads to retarded early mouse embryo development and altered carbohydrate utilisation by the blastocyst. *Reprod Fertil Dev* 2012; **24**:804–812.
11. Bakos HW, Mitchell M, Setchell BP, Lane M. The effect of paternal diet-induced obesity on sperm function and fertilization in a mouse model. *Int J Androl* 2011; **34**:402–410.
12. Chavarro JE, Toth TL, Wright DL, Meeker JD, Hauser R. Body mass index in relation to semen quality, sperm DNA integrity, and serum reproductive hormone levels among men attending an infertility clinic. *Fertil Steril* 2010; **93**:2222–2231.
13. Hammoud AO, Wilde N, Gibson M, Parks A, Carrell DT, Meikle AW. Male obesity and alteration in sperm parameters. *Fertil Steril* 2008; **90**:2222–2225.
14. Donkin I, Versteyhe S, Ingerslev LR, Qian K, Mechta M, Nordkap L, Mortensen B, Appel EV, Jorgensen N, Kristiansen VB, Hansen T, Workman CT *et al.* Obesity and bariatric surgery drive epigenetic variation of spermatozoa in humans. *Cell Metab* 2016; **23**: 369–378.
15. Chen Q, Yan M, Cao Z, Li X, Zhang Y, Shi J, Feng G, Peng H, Zhang X, Zhang Y, Qian J, Duan E *et al.* Sperm tsRNAs contribute to intergenerational inheritance of an acquired metabolic disorder. *Science* 2016; **351**:397–400.
16. Fowden AL, Coan PM, Angiolini E, Burton GJ, Constancia M. Imprinted genes and the epigenetic regulation of placental phenotype. *Prog Biophys Mol Biol* 2011; **106**:281–288.
17. McPherson NO, Bell VG, Zander-Fox DL, Fullston T, Wu LL, Robker RL, Lane M. When two obese parents are worse than one! Impacts on embryo and fetal development. *Am J Physiol Endocrinol Metab* 2015; **309**:E568–E581.
18. Binder NK, Beard SA, Kaitu'u-Lino TJ, Tong S, Hannan NJ, Gardner DK. Paternal obesity in a rodent model affects placental gene expression in a sex-specific manner. *Reproduction* 2015; **149**: 435–444.
19. Mitchell M, Strick R, Strissel PL, Dittrich R, McPherson NO, Lane M, Pliushch G, Potabattula R, Haaf T, El Hajj N. Gene expression and epigenetic aberrations in F1-placentas fathered by obese males. *Mol Reprod Dev* 2017; **84**:316–328.
20. Bar J, Kovo M, Schraiber L, Shargorodsky M. Placental maternal and fetal vascular circulation in healthy non-obese and metabolically healthy obese pregnant women. *Atherosclerosis* 2017; **260**: 63–66.
21. Jauniaux E, Watson AL, Hempstock J, Bao Y, Skepper JN, Burton GJ. Onset of maternal arterial blood flow and placental oxidative stress. *Am J Pathol* 2000; **157**:2111–2122.
22. Malhotra JD, Kaufman RJ. The endoplasmic reticulum and the unfolded protein response. *Semin Cell Dev Biol* 2007; **18**: 716–731.
23. Westermeier F, Saez PJ, Villalobos-Labra R, Sobrevia L, Farias-Jofre M. Programming of fetal insulin resistance in pregnancies with maternal obesity by ER stress and inflammation. *Biomed Res Int* 2014; **2014**:1–13.
24. Cavallari JF, Fullerton MD, Duggan BM, Foley KP, Denou E, Smith BK, Desjardins EM, Henriksbo BD, Kim KJ, Tuinema BR, Stearns JC, Prescott D *et al.* Muramyl dipeptide-based postbiotics mitigate obesity-induced insulin resistance via IRF4. *Cell Metab* 2017; **25**:1063–1074.e3.
25. Marcinko K, Sikkema SR, Samaan MC, Kemp BE, Fullerton MD, Steinberg GR. High intensity interval training improves liver and adipose tissue insulin sensitivity. *Mol Metab* 2015; **4**:903–915.
26. Matthews DR, Hosker JP, Rudenski AS, Naylor BA, Treacher DF, Turner RC. Homeostasis model assessment: insulin resistance and beta-cell function from fasting plasma glucose and insulin concentrations in man. *Diabetologia* 1985; **28**:412–419.
27. Yamaguchi M, Ogren L, Endo H, Thordarson G, Bigsby RM, Talamantes F. Production of mouse placental lactogen-I and placental lactogen-II by the same giant cell. *Endocrinology* 1992; **131**: 1595–1602.
28. Campbell JM, Lane M, Owens JA, Bakos HW. Paternal obesity negatively affects male fertility and assisted reproduction outcomes: a systematic review and meta-analysis. *Reprod Biomed Online* 2015; **31**:593–604.
29. Pearce KL, Hill A, Tremellen KP. Obesity related metabolic endotoxemia is associated with oxidative stress and impaired sperm DNA integrity. *Basic Clin Androl* 2019; **29**:6.
30. Krock BL, Skuli N, Simon MC. Hypoxia-induced angiogenesis: good and evil. *Genes Cancer* 2011; **2**:1117–1133.
31. Harris SE, Matthews KSH, Palaiologou E, Tashev SA, Lofthouse EM, Pearson-Farr J, Goggin P, Chatelet DS, Johnston DA, Jongen MS, Page AM, Cleal JK *et al.* Pericytes on placental capillaries in terminal villi preferentially cover endothelial junctions in regions furthest away from the trophoblast. *Placenta* 2021; **104**:1–7.
32. Ohlsson R, Falck P, Hellstrom M, Lindalh P, Bostrom H, Franklin G, Ahrlund-Richter L, Pollard J, Soriano P, Betsholtz C. PDGFB regulates the development of the labyrinthine layer of the mouse fetal placenta. *Dev Biol* 1999; **212**:124–136.
33. Hu X, Li J, Zhang Q, Zheng L, Wang G, Zhang X, Zhang J, Gu Q, Ye Y, Guo S-W, Yang X, Wang L. Phosphoinositide 3-Kinase (PI3K) subunit p110δ is essential for trophoblast cell differentiation and placental development in mouse. *Sci Rep* 2016; **6**:28201. doi: 10.1038/srep28201.
34. Iwawaki T, Akai R, Yamanaka S, Kohno K. Function of IRE1 alpha in the placenta is essential for placental development and embryonic viability. *PNAS* 2009; **106**:16657–16662.
35. Charnock-Jones DS. Placental hypoxia, endoplasmic reticulum stress and maternal endothelial sensitisation by sFLT1 in pre-eclampsia. *J Reprod Immunol* 2016; **114**:81–85.
36. Smith JA. Regulation of cytokine production by the unfolded protein response; implications for infection and autoimmunity. *Front Immunol* 2018; **9**:422. doi: 10.3389/fimmu.2018.00422.
37. Soubry A, Schildkraut JM, Murtha A, Wang F, Huang Z, Bernal A, Kurtzberg J, Jirtle RL, Murphy SK, Hoyo C. Paternal obesity is associated with IGF2hypomethylation in newborns- results from a Newborn Epigenetics Study (NEST) cohort. *BMC Med* 2013; **11**:29.
38. Wu J, Zhu AX. Targeting insulin-like growth factor axis in hepatocellular carcinoma. *J Hematol Oncol* 2011; **4**:30.
39. Street ME, Viani I, Ziveri MA, Volta C, Smerieri A, Bernasconi S. Impairment of insulin receptor signal transduction in placentas of intra-uterine growth-restricted newborns and its relationship with fetal growth. *Eur J Endocrinol* 2011; **164**:45–52.
40. Newbern D, Freemark M. Placental hormones and the control of maternal metabolism and fetal growth. *Curr Opin Endocrinol Diabetes Obes* 2011; **18**:409–416.

41. Lau HH, Ng NHJ, Loo LSW, Jasmen JB, Teo AKK. The molecular functions of hepatocyte nuclear factors - In and beyond the liver. *J Hepatol* 2018; **68**:1033–1048.
42. Park S, Jang A, Bouret SG. Maternal obesity-induced endoplasmic reticulum stress causes metabolic alterations and abnormal hypothalamic development in the offspring. *PLoS Biol* 2020; **18**:e3000296.
43. Perez-Arancibia R, Rivas A, Hetz C. (off)Targeting UPR signaling: the race toward intervening ER proteostasis. *Expert Opin Ther Targets* 2018; **22**:97–100.
44. Soares Moretti AI, Martins Laurindo FR. Protein disulfide isomerases: redox connections in and out of the endoplasmic reticulum. *Arch Biochem Biophys* 2017; **617**:106–119.
45. Speakman JR. Measuring energy metabolism in the mouse - theoretical, practical, and analytical considerations. *Front Physiol* 2013; **4**:34.
46. Ahn H, Park J, Gilman-Sachs A, Kwak-Kim J. Immunologic characteristics of preeclampsia, a comprehensive review. *Am J Reprod Immunol* 2011; **65**:377–394.
47. Shweiki D, Itin A, Soffer D, Keshet E. Vascular endothelial growth factor induced by hypoxia may mediate hypoxia-initiated angiogenesis. *Nature* 1992; **359**:843–845.
48. Ghosh R, Lipson KL, Sargent KE, Mercurio AM, Hunt JS, Ron D, Urano F. Transcriptional regulation of VEGF-A by the unfolded protein response pathway. *PLoS One* 2010; **5**: e9575.
49. Pereira ER, Frudd K, Awad W, Hendershot LM. Endoplasmic reticulum (ER) stress and hypoxia response pathways interact to potentiate hypoxia-inducible factor 1 (HIF-1) transcriptional activity on targets like vascular endothelial growth factor (VEGF). *J Biol Chem* 2014; **289**:3352–3364.
50. Broere-Brown ZA, Schalekamp-Timmermans S, Hofman A, Jaddoe V, Steegers E. Fetal sex dependency of maternal vascular adaptation to pregnancy: a prospective population-based cohort study. *BJOG* 2016; **123**:1087–1095.
51. Taylor BD, Ness RB, Klebanoff MA, Tang G, Roberts JM, Hougaard DM, Skogstrand K, Haggerty CL. The impact of female fetal sex on preeclampsia and the maternal immune milieu. *Pregnancy Hypertens* 2018; **12**:53–57.
52. Global Pregnancy C, Schalekamp-Timmermans S, Arends LR, Alsaker E, Chappell L, Hansson S, Harsem NK, Jalmby M, Jeyabalan A, Laivuori H, Lawlor DA, Macdonald-Wallis C *et al.* Fetal sex-specific differences in gestational age at delivery in pre-eclampsia: a meta-analysis. *Int J Epidemiol* 2017; **46**: 632–642.
53. Aljunaidy MM, Morton JS, Cooke CM, Davidge ST. Prenatal hypoxia and placental oxidative stress: linkages to developmental origins of cardiovascular disease. *Am J Physiol Regul Integr Comp Physiol* 2017; **313**:R395–R399.
54. Zhang Z, Grewer C. The sodium-coupled neutral amino acid transporter SNAT2 mediates an anion leak conductance that is differentially inhibited by transported substrates. *Biophys J* 2007; **92**:2621–2632.
55. Manta-Vogli PD, Schulpis KH, Dotsikas Y, Loukas YL. The significant role of amino acids during pregnancy: nutritional support. *J Matern Fetal Neonatal Med* 2020; **33**:334–340.
56. Morotti M, Bridges E, Valli A, Choudhry H, Sheldon H, Wigfield S, Gray N, Zois CE, Grimm F, Jones D, Teoh EJ, Cheng WC *et al.* Hypoxia-induced switch in SNAT2/SLC38A2 regulation generates endocrine resistance in breast cancer. *Proc Natl Acad Sci U S A* 2019; **116**:12452–12461.
57. Sferruzzi-Perri AN, Sandovici I, Constancia M, Fowden AL. Placental phenotype and the insulin-like growth factors: resource allocation to fetal growth. *J Physiol* 2017; **595**:5057–5093.
58. Forbes K, Westwood M, Baker PN, Aplin JD. Insulin-like growth factor I and II regulate the life cycle of trophoblast in the developing human placenta. *Am J Physiol-Cell Physiol* 2008; **294**:C1313–C1322.
59. Lassance L, Miedl H, Absenger M, Diaz-Perez F, Lang U, Desoye G, Hiden U. Hyperinsulinemia stimulates angiogenesis of human fetoplacental endothelial cells: a possible role of insulin in placental hypervascularization in diabetes mellitus. *J Clin Endocrinol Metabol* 2013; **98**:E1438–E1447.
60. Sferruzzi-Perri AN, Owens JA, Pringle KG, Robinson JS, Roberts CT. Maternal insulin-like growth factors-I and -II act via different pathways to promote fetal growth. *Endocrinology* 2006; **147**: 3344–3355.
61. de Almeida-Faria J, Duque-Guimarães DE, Ong TP, Pantaleão LC, Carpenter AA, Loche E, Kusinski LC, Ashmore TJ, Antrobus R, Bushell M, Fernandez-Twinn DS, Ozanne SE. Maternal obesity during pregnancy leads to adipose tissue ER stress in mice via miR-126-mediated reduction in Lunapark. *Diabetologia* 2021; **64**: 890–902.
62. Ornellas F, Souza-Mello V, Mandarim-de-Lacerda CA, Aguila MB. Programming of obesity and comorbidities in the progeny: lessons from a model of diet-induced obese parents. *PLoS One* 2015; **10**:e0124737.
63. Kalhan S, Parimi P. Gluconeogenesis in the fetus and neonate. *Semin Perinatol* 2000; **24**:94–106.
64. Deodati A, Argemi J, Germani D, Puglianiello A, Alisi A, De Stefanis C, Ferrero R, Nobili V, Aragon T, Cianfarani S. The exposure to uteroplacental insufficiency is associated with activation of unfolded protein response in postnatal life. *PLoS One* 2018; **13**:e0198490.